Fold localisation at pre-existing normal faults: Field observations and analogue modelling of the Achental structure, Northern Calcareous Alps, Austria

Willemijn Sarah Maria Theresia van Kooten[1,2], Hugo Ortner[1], Ernst Willingshofer[3], Dimitrios Sokoutis[3,4], Alfred Gruber[5], Thomas Sausgruber[6]

[1]Institut für Geologie, Universität Innsbruck, Innsbruck, 6020, Austria
[2]Department of Digital Business & Software Engineering, MCI - The Entrepreneurial School, Innsbruck, 6020, Austria
[3]Department of Earth Sciences, Utrecht University, Utrecht, 3584 CB, Netherlands
[4]Department of Geosciences, University of Oslo, Oslo, Norway
[5]Geologische Bundesanstalt für Österreich (GBA), Wien, 1030, Austria
[6]die.wildbach, Wilhelm-Greil-Straße 9 6020 Innsbruck, Austria

Correspondence to: Willemijn S.M.T. van Kooten (willemijn.vankooten@mci.edu), ORCID: 0000-0002-9784-444X

Abstract

Within the Northern Calcareous Alps fold-and-thrust belt of the Eastern Alps, multiple pre-shortening deformation phases have contributed to the structural grain that controlled localisation of deformation at later stages. In particular, Jurassic rifting and opening of the Alpine Tethys led to the formation of extensional basins at the northern margin of the Apulian plate. Subsequent Cretaceous shortening within the Northern Calcareous Alps produced the enigmatic Achental structure, which forms a sigmoidal transition zone between two E–W striking major synclines. One of the major complexities of the Achental structure is that all structural elements are oblique to the Cretaceous direction of shortening. Its sigmoidal form was, therefore, proposed to be a result of forced folding at the boundaries of the Jurassic Achental basin. This study analyses the structural evolution of the Achental structure through integrating field observations with crustal-scale physical analogue modelling, to elucidate the influence of pre-existing crustal heterogeneities on oblique basin inversion. From brittle-ductile models that include a weak basal décollement, we infer that oblique shortening of pre-existing extensional faults can lead to the localisation of deformation at the pre-existing structure and predicts thrust and fold structures that are consistent with field observations. Consequently, the Achental low-angle thrust and sigmoidal fold train was able to localise at the former Jurassic basin margin, with a vergence opposite to the controlling normal fault, creating the characteristic sigmoidal morphology during a single phase of NW-directed shortening.

1 Introduction

The deformational style and tectonic history of Earth's orogenic belts is strongly influenced by pre-existing structural elements. In particular, structures formed by shortening and inversion of pre-orogenic basins are often governed by the reactivation of former basin-bounding normal faults as summarised by Turner and Williams (2004) or Cooper and Warren (2020). Consequently, previous studies have focused on the mechanics of fault reactivation (e.g., Sibson, 1995; Etheridge, 1986; Tong and Yin, 2011; Nielsen and Hansen, 2000), or present regional case studies of basin inversion (e.g., Kley et al., 2005; Thorwart et al., 2021; Héja et al., 2022). Existing literature presenting analogue and numerical modelling of inversional settings is extensive and includes the reactivation of planar and listric extensional fault systems of various orientation as well as basin inversion orthogonal or oblique to the basin axes (e.g., Bonini, 1998; Buiter and Pfiffner, 2003; Amilibia et al., 2005; Buchanan and McClay, 1992; Koopman et al., 1987; Konstantinovskaya et al., 2007; Sassi et al., 1993; Dubois et al., 2002; Zwaan et al., 2022; Brun and Nalpas, 1996). In most models, newly formed reverse faults are synthetic to the pre-existing normal faults (see

also Bonini et al., 2012: their Fig.~~ure~~ 3), whereas the formation of thrust faults antithetic to the former basin-bounding faults is seldomly described.

In this study, we use an example from the Northern Calcareous Alps (NCA) in Austria (Fig.~~ure~~ 1), in which basin inversion during Alpine orogeny has created a low-angle thrust antithetic to a normal fault bounding a Jurassic extensional basin. In the hanging wall of this thrust, a fold train outlines the margins of this basin, forming a characteristic sigmoidal shape that has been the subject of geological investigations since the beginning of the 20th century (Ampferer, 1902, 1941; Fuchs, 1944; Nagel, 1975; Nagel et al., 1976; Quenstedt, 1933). We use the example of the Achental structure and its underlying basin geometry as a starting point for analogue modelling, to simulate the oblique inversion of a former extensional basin and the deformation of a brittle-ductile sedimentary succession at its margins. The main aim of this study is to better understand strain localization and associated deformation by folding and thrusting at oblique basin bounding faults. In particular, this study examines whether a sigmoidal hanging wall shape outlining former basin margins can be explained by a single phase of oblique shortening and if so what are the critical rheological and kinematic parameters to obtain such structures. Our modelling results are then compared to the Achental structure, to better understand the formation of complex inversion structures in fold-and-thrust belts.
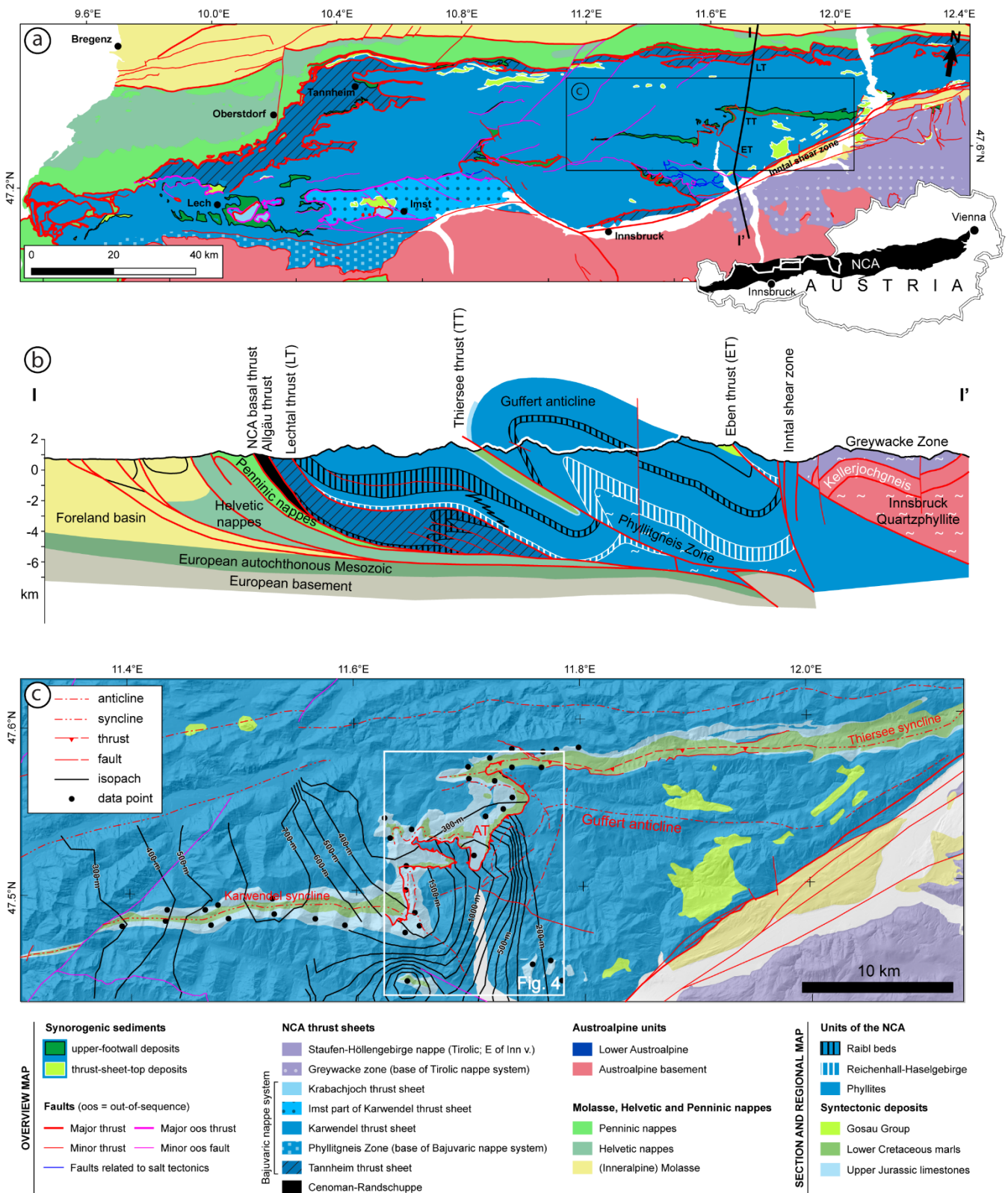
Figure 1: (a) Map showing the main tectonic units of W-Austria. Inset shows~~Tectonic map showing~~ the location of the Northern Calcareous Alps in ~~western~~ Austria. Rectangles shows location of ~~Figure~~ Fig. 1c. Modified after Ortner and Kilian (2022). (b) N–S cross-section of the NCA at ~ 11.7°E, crossing the Achental structure. (c) Geological map of the Achental structure within the Karwendel thrust sheet. Black lines show isopachs of the Upper Jurassic Oberalm Fm, with data compiled from Nagel et al. (1976) and Schütz (1979). The hanging wall and footwall of the Achental thrust (AT) were contoured separately, single outliers in the data were ignored. Major thickness changes occur from W to E ~~and,~~ a maximum is observed in the southern hanging wall of the thrust. Rectangle shows the location of the study area (Fig. 4).

2 Geological setting

The Northern Calcareous Alps (NCA) of Austria have a polyphase tectonic and sedimentary history that started in the Permian. The following evolutionary stages are distinguished (Figure 2):

1) Deposition of a Permian–Triassic carbonate platform succession on the south(east)ern passive margin of Pangaea bordering the Neotethys from the Permian to the end of the Triassic (e.g., Haas et al., 1995; Lein, 1987; Schmid et al., 2004; Stampfli et al., 1998; Schmid et al., 2008) (Figure 2a).

2) Early to Middle Jurassic rifting and subsequent opening of the Alpine Tethys that separated the Apulian/Adriatic microplate from the European continent led to subsidence and drowning of the Triassic carbonate platforms (e.g., Faupl and Wagreich, 1999; Schmid et al., 2004; Froitzheim and Manatschal, 1996) (Figure 2b). Rift-related faulting established the normal faults that were inverted during Cretaceous orogeny (Eberli et al., 1993; Ortner et al., 2008).

3) Shortening related to Late Jurassic obduction of Neotethys oceanic crust onto the southeastern Apulian margin heralded inversion of this margin, which culminated in the Cretaceous orogeny (Schmid et al., 2004; Stüwe and Schuster, 2010) (Figure 2c). During the Cretaceous orogeny the NCA were a typical thin-skinned fold-and-thrust belt at the external margin of the Austroalpine orogenic wedge in lower plate position (Eisbacher and Brandner, 1996; Ortner and Kilian, 2022).

4) During the Late Cretaceous this wedge was transported toward the northwestern passive margin of the Apulian plate, which became an active margin through subduction of the Alpine Tethys (Ortner and Sieberer, 2022; Stüwe and Schuster, 2010; Willingshofer et al., 1999).

5) Late Eocene closure of the Alpine Tethys caused collision between the lower, European and upper, Apulian plates and thus a second, Paleogene phase of mountain building, referred to as "Alpine orogeny" (Eisbacher and Brandner, 1996; Schmid et al., 2004; Stüwe and Schuster, 2010; Ortner, 2003a). In the course of this process the Austroalpine units and the NCA fold-and-thrust belt were transported piggyback onto the European margin. Contrasting with Cretaceous orogeny, the Austroalpine wedge formed the upper plate during Paleogene orogeny.
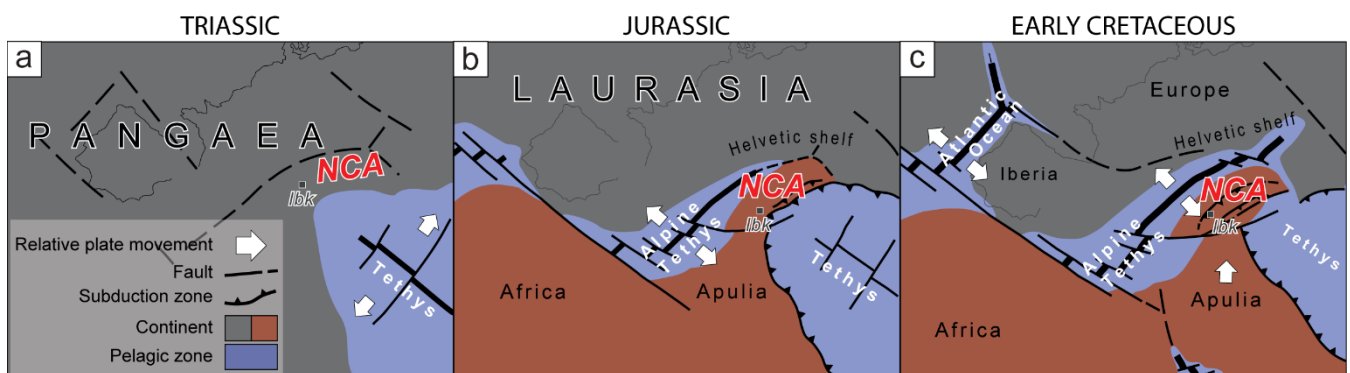
Figure 2: Developmental stages in the tectonic evolution of the Northern Calcareous Alps, modified after Schuster et al. (2019). (a) (Permo)triassic stage with sedimentation on the passive margin of Pangaea. (b) Early–Middle Jurassic opening of the Alpine Tethys, with sedimentation in basins and on swells. (c) Cretaceous orogeny. The present-day location of Innsbruck (Ibk) is marked.

Relevant for this study are the Jurassic rifting that created sedimentary basins and the Cretaceous and Paleogene shortening that led to basin inversion. Jurassic extensional basins formed along intersecting fault systems with N–S trending normal faults and E–W trending transform faults, as documented in the Eastern Alps of Switzerland (Eberli, 1987, 1985; Weissert and Bernoulli, 1985). Similar orientations of extensional normal faults have been found in the Western Alps (Lemoine et al., 1986). The existence of an extensional basin in the Achensee region is indicated by filled fissures that occur in Oberrhät limestone (Gruber et al., 2022), strong lateral thickness variations of (Upper) Jurassic strata (Figure 1b) (Schütz, 1979; Nagel et al., 1976) and characteristic breccias that are locally intercalated in basinal Jurassic sediments (Spieler and Brandner, 1989; Channell et al., 1992; Channell et al., 1990; Brandner et al., 2011). Cretaceous to Paleogene shortening within the NCA is

95   characterized by two separate directions of transport. During Cretaceous orogeny the thrust sheets of the NCA were transported
      and stacked in WNW- to NW-direction (Eisbacher and Brandner, 1996), whereas Paleogene shortening of the NCA fold-and-
      thrust belt was associated with N- to NNE transport directions (Schmid et al., 1996). These differences are well documented
      within the basement units of the Austroalpine wedge (Froitzheim et al., 1994), although synorogenic growth strata show
      continuous shortening within the NCA (Ortner, 2001, 2003b; Ortner and Gaupp, 2007; Ortner et al., 2016).

100   **2.1 Sedimentary succession**

      The sedimentary succession of the NCA encompasses a late Permian to Oligocene stratigraphy. The Permotriassic succession
      reflects subsidence of the south(east)ern passive margin of Pangaea from continental to shallow marine conditions. During the
      Permian–Middle Triassic, the marine ingression of the Tethys led to the formation of a subtidal-supratidal marine environment,
      where the evaporitic Haselgebirge-Reichenhall succession accumulated. The Haselgebirge contains large amounts of halite,
105   gypsum and anhydrite in a shale matrix (Leitner and Neubauer, 2011). The thickness of Haselgebirge is highly variable, due
      to salt tectonics and solution, but a primary thickness of 500–1000 m can be expected (Spötl, 1989: their Fig. 2). Lower Triassic
      sandstones (Alpine Buntsandstein) overlie the Haselgebirge and are followed by an Anisian limestone-dolostone-evaporite
      succession (Reichenhall Formation (Fm; Fig. 3)) with a thickness of 80–200 m in the Achensee region (Nagel et al., 1976).
      The Haselgebirge-Reichenhall succession represents a rheologically incompetent part of the stratigraphic column, forming the
110   principal décollement of the NCA (Eisbacher and Brandner, 1995). The Eben thrust (Fig. 1a, b) brings the Haselgebirge-
      Reichenhall succession to the surface in the Achensee region. Its presence in the subsurface has been inferred from depth-
      extrapolated cross sections based on TRANSALP and industry reflection seismic lines (Auer and Eisbacher, 2003: their Fig.
      15).

      The evaporitic Haselgebirge-Reichenhall succession transitions into a succession of Anisian–Ladinian limestones (Alpine
115   Muschelkalk Group; Bechstädt and Mostler, 1974). These vary from shallow-water, strongly bioturbated mud- to wackestones
      (e.g., Virgloria Fm, Steinalm Fm) to basin marginal and basinal limestones (Reifling Fm; Rüffer and Zühlke, 1995). The
      uppermost Alpine Muschelkalk Group interfingers with the Wetterstein limestone (Anisian–Carnian), which forms the first of
      two major carbonate platforms of the NCA (Fig. 3). Although the Alpine Muschelkalk Group and Wetterstein limestone
      show a general thickness between 1000 to > 2200 m in the Achensee region (Sausgruber, 1994b; Nagel et al., 1976; Gruber et
120   al., 2022), cross sections in Gruber et al. (2022) show a thickness up to 3500 m. These thickness variations might be a result
      of salt tectonics in the Triassic (e.g., Ortner and Kilian, 2022; Granado et al., 2019; Kilian et al., 2021), however, minibasin
      margins with typical stratal geometries such as wedges or hooks (Giles and Rowan, 2012) or flaps (Rowan et al., 2016) have
      not been documented in the Achensee region so far. About 400 m of Carnian sandstones, shales, dolomites, evaporites and
      limestones (Raibl beds) overlie the Wetterstein platform unconformably (Gruber et al., 2022; Krainer et al., 2011; Sausgruber,
125   1994a; Jerz, 1966). Norian dolomites (Hauptdolomit carbonate platform) (Müller-Jungbluth, 1968; Fruth and Scherreiks, 1982;
      Zorlu, 2007) form the second major platform of the NCA, which is again 1–2 km thick (Donofrio et al., 2003). The
      Hauptdolomit platform subsequently drowns towards its top; a Norian succession of alternating limestones and dolostones
      (Plattenkalk; Gümbel, 1861) heralds the deposition of Rhaetian basinal shales (Kössen Fm), which interfinger with Upper
      Rhaetian platform carbonates (Oberrhät limestone; Riedel, 1988; Golebiowski, 1991) (Fig. 3). The Ladinian and Norian
130   platforms represent an approximately 3 km thick, mechanically competent unit. The mechanical significance of intervening
      Carnian shales and evaporites for deformation during the Cretaceous orogeny has been previously discussed (Kilian et al.,
      2021) and approached through analogue modelling in this contribution (see Section 3.2 and 4 below).

      While rifting of the Alpine Tethys (Eberli et al., 1993) in the Jurassic caused subsidence and drowning of the Triassic carbonate
      platforms (Ortner et al., 2008), rotational block faulting caused by the extensional movement (Lackschewitz et al., 1991)
135   resulted in a differentiation of basin and swell facies (Nagel et al., 1976; Spieler and Brandner, 1989). Early Jurassic red

condensed limestones (e.g., Adnet Fm, Sinemurian–Toarcian; Sausgruber, 1994a; Spieler, 1994); were deposited on swells, and basinal strata (e.g., Allgäu Fm. Hettangian–Oxfordian) in subsided areas (Brandner and Gruber, 2011: their Fig. 15). Basins and swells existed until the Middle–Late Jurassic (Brandner and Gruber, 2011; Ortner et al., 2008; Ortner and Kilian, 2016; Spieler and Brandner, 1989). The continental margin reached its maximum subsidence in the Oxfordian (Ortner and Kilian, 2016), when radiolarites were deposited (Ruhpolding radiolarite) (Nagel et al., 1976; Sausgruber, 1994a; Bernoulli and Jenkyns, 1974). The overlying Late Jurassic–Early Cretaceous (Kimmeridgian–Berriasian) stratigraphic succession (e.g., Oberalm and Schrambach Fms) testifies to a shallowing depositional environment (Gruber et al., 2022; Gawlick, 2004; Kilian, 2013; Sausgruber, 1994a; Gümbel, 1861; Lipold, 1854). The lower–middle Jurassic succession has a mean thickness of 290 m (based on cross sections and compilations of Ortner and Gruber, 2011; Sausgruber, 1994b; Spieler, 1995; Auer, 2001; Gruber, 2011), while the upper Jurassic to lower Cretaceous pelagic limestones (Oberalm Fm) reach a thickness of more than 1300 m and cover the pre-existing relief (Nagel et al., 1976).

Increased influx of siliciclastic detritus, beginning in the Early Cretaceous, marks the onset of synorogenic sedimentation, commencing with the Schrambach Fm (Berriasian–Aptian), consisting of marls and intercalated calcareous and turbiditic sandstones (Lipold, 1854; Ortner, 2003b). In the western Thiersee syncline, its thickness is ~ 300–400 m (Ortner and Gruber, 2011; Schütz, 1979), thinning to ~ 150 m east of Achenkirch (Ortner and Gruber, 2011). The overlying synorogenic sediments of the Gosau Group (Late Cretaceous to Paleogene) complete the stratigraphic succession of the Achental region (Ortner, 2003b).
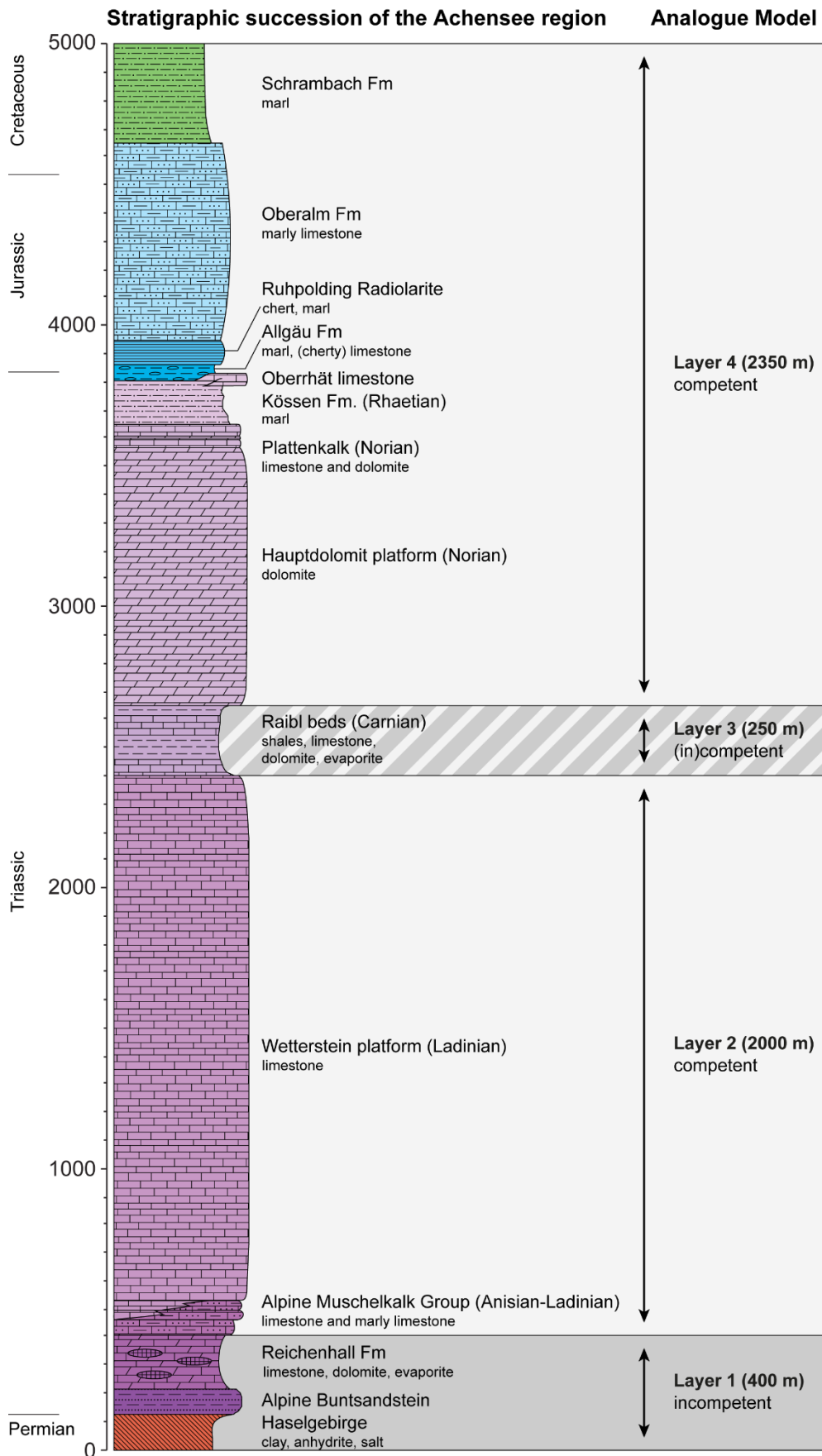
Figure 3: Stratigraphic overview of the Permian–Cretaceous sedimentary succession of the Karwendel thrust sheet in the Achensee area. ~~M~~ modified after Kilian et al. (2021). Various sedimentary strata have been assigned to different incompetent and competent layers (1–4) in the analogue model set-up (see also Fig. 6). The Raibl beds were modelled as incompetent or competent, depending on the specific model. Kilian et al. (2021) discuss the rheological behaviour of the Raibl beds in more detail.

2.2 Achental structure

The Achental structure is located within the Karwendel thrust sheet, following the revised nappe structure of the NCA (Ortner, 2016; Ortner and Kilian, 2022; Kilian and Ortner, 2019), and geographically surrounds the Achensee in Tyrol, Austria (Fig. 1, 4). The structure is characterized by the low-angle Achental thrust, which separates the Karwendel and Thiersee synclines in its footwall, from the Guffert-Unnutz-Montscheinspitze anticline fold train in its hanging wall. It forms a structural NNE–SSW striking transfer zone between Karwendel and Thiersee synclines. The Achental thrust reaches into the cores of these folds and gradually loses offset toward the NE and SW (Ortner and Gruber, 2011). The thrust changes its orientation and stratigraphic offset throughout the Achental structure; in the north (Mahmooskopf-Natterwand section, Fig. 4), the thrust strikes E–W and dips ~ 23–30° south (Ortner, 2003b and Beer, 2003, respectively) with a total displacement of ~ 5–7 km (Auer and Eisbacher, 2003 and Ortner, 2003b, respectively), based on cut-offs of Jurassic strata in Section B (Fig. 5b). In the central section, the thrust strikes NNE–SSW and dips 15° SE (Spieler, 1994). The maximum stratigraphic offset of ~ 8 km (Eisbacher and Brandner, 1996) is located NE of Achenkirch, where Hauptdolomit (Norian) is thrusted onto Schrambach Fm (Early Cretaceous) (Fig. 4, 5a) (Gruber et al., 2022). In the south, the Achental thrust dips SE, offsets the hinge of the Seebergspitze syncline and runs into the core of the Karwendel syncline (Fig. 4). Although it separates consecutive Late Jurassic–Early Cretaceous strata, the contrasting orientation of the strata (E-dipping north of the Seebergspitze syncline hinge; vertical to S-dipping west of the hinge) rules out a stratigraphic contact between these formations (Ortner and Gruber, 2011). However, offset is minor and dies out not much further to the west. A series of km-scale, E–W striking north-vergent synclines (Karwendel, Gröben, Großzemmalm, Klammbach and Thiersee synclines) and associated anticlines (Scharfreuter and Hofjoch anticlines) form the footwall of the Achental thrust (Fig. 4). These folds are overridden by the Achental and Leiten thrust (Ortner and Gruber, 2011: their Fig. 2).

The hanging wall of the Achental thrust ("Achentaler Schubmasse" after Quenstedt (1933)) is comprised of the connected Montscheinspitze, Unnutz and Guffert anticlines (Fig. 4, 5), which change strike approximately parallel to the Achental thrust. West of the Achental structure, the Montscheinspitze anticline is connected to the Karwendel syncline (Ampferer and Heissel, 1950: their section 3). In the SW corner of the Achental structure, the northern anticline limb is folded with the Seebergspitze syncline into an overturned position (Fuchs, 1944; Ortner and Gruber, 2011). The Achental thrust emplaces the anticline limb onto the Karwendel syncline (Nagel et al., 1976). The Unnutz anticline, a recumbent fold with a SE-dipping axial surface and an increasingly SSW-plunging fold axis (From N–S: 205/18, 200/27 and 187/23; Ortner and Gruber, 2011), forms the N–S striking part of the fold train. The Unnutz anticline (Fig. 5a) resembles a dome, rather than a cylindrical fold (e.g., Mojsisovics, 1871; Sausgruber, 1994a, 1994b; Ortner and Gruber, 2011). NE of Achenkirch, the Unnutz anticline is folded around the Rotmöserkopf synform and continues as the E–W striking Guffert anticline (Gruber et al., 2022; Ortner and Gruber, 2011) (Fig. 4, 5b). The Guffert anticline has a S-dipping axial surface, sub-horizontal fold axis with ESE–WNW strike and an overturned northern limb.

The characteristic sigmoidal shape of the Guffert-Unnutz-Montscheinspitze anticline fold train has been noticed since the beginning of the 20th century (Ampferer, 1902) and is one of the greatest complexities in the geologic interpretation of the Achental structure. Over the past century, four principal hypotheses have been developed to explain its formation (see also Ortner and Gruber, 2011; Gruber et al., 2022). These include *1)* bending of an originally E–W striking anticline due to rotational movements (e.g., Ampferer, 1921; Auer, 2001; Spengler, 1953, 1956; Ampferer, 1941); *2)* passive dragging of the central part of the structure, caused by a larger amount of shortening in the eastern part of the structure, compared to its western part (Nagel, 1975); *3)* polyphase deformation, in which a former W-directed thrust (Achental thrust) was reactivated by N-directed thrusting (Fuchs, 1944; Channell et al., 1992; Channell et al., 1990; Ortner, 2003b; Spieler and Brandner, 1989), and *4)* forced folding of the Guffert-Unnutz-Montscheinspitze fold train at the border of a carbonate platform, or along an inverted Jurassic normal fault (Eisbacher and Brandner, 1995, 1996; Ortner and Gruber, 2011).

The kinematic history of the Achental structure is characterised by polyphase shortening (Fuchs, 1944; Spieler and Brandner, 1989; Ortner, 2003b; Ortner and Gruber, 2011). Barremian sediments below the Achental thrust indicate an Early Cretaceous maximum age of thrusting. The oldest contractional deformation in the area is indicated by an angular unconformity in both limbs of the Guffert anticline at the base of the Gosau Group (Ortner and Gruber, 2011), indicating Early Cretaceous growth of the anticline. Anticlines grow on top of décollements, therefore we speculate that the Achental thrust was already active at this time. Cretaceous shortening along the Achental thrust is evident from calcite slickensides showing NNW- to NW-directed movement (Eisbacher & Brandner, 1995, 1996; Sausgruber, 1994a, 1994b). This phase of shortening caused an initial uplift and tightening of the Unnutz-Achental structure and is responsible for NW-striking high-angle dextral transfer faults, which segment the Unnutz anticline (Eisbacher and Brandner, 1995, 1996). Late Cretaceous to Paleogene (80–30 Ma) NE-directed shortening superimposed existing folds and fault movement, reactivating pre-existing NW-striking transfer faults and forming NW-plunging folds and NE-striking high-angle transfer faults (Eisbacher and Brandner, 1995). As a result, three major fold orientations are recognized in the Achensee region (Sausgruber, 1994a). Folds with NE–SW striking fold axes formed during NW-directed, pre-Gosau contraction. E–W striking fold axes formed during N-directed shortening and NW–SE striking fold axes formed during NE-directed shortening. Folding of the Achental and Leiten thrust around the E–W striking Roßstand anticline, but not around the parallel Scharfreuter anticline (Sausgruber, 1994b; Ortner and Gruber, 2011: their Fig. 2) (Figure 4) suggests that the thrust is older than the general N-directed shortening (Spieler and Brandner, 1989). However, since the oldest sediments covering both the hanging wall and footwall of the northern Achental thrust belong to the Gosau Group, N-directed shortening must have occurred post-Gosau (Ortner, 2003b), post-dating the formation of the western Achental thrust. Neogene folds superimpose older folding and can be found e.g., within the Thiersee syncline (Sausgruber, 1994b). Fold interference creates intriguing dome-and-basin structures that complicate the geological interpretation of the Achental structure. Polyphase deformation of the Achental structure is visible from field evidence, showing refolded faults and fold axes (e.g., Gruber et al., 2022; Ortner and Gruber, 2011; Sausgruber, 1994b). However, it is unclear whether two phases of deformation were necessary to create the Achental structure (Gruber et al., 2022).

A link between the Jurassic basin architecture and the present-day sigmoidal form of the Achental structure has been proposed previously, suggesting that the latter is the result of forced folding (Eisbacher and Brandner, 1995, 1996; Ortner and Gruber, 2011) that depended on pre-existing extensional structures rather than the exact direction of shortening (Töchterle, 2005). Channell et al. (1990) postulated the existence of an E–W striking sinistral pull-apart basin, forming a controlling inherited Jurassic basin-and-swell topography. This is supported by field observations: Cretaceous transport directions (Sausgruber, 1994a, 1994b; Ortner and Gruber, 2011) are oblique to the axis of the Karwendel and Thiersee synclines. If deformed within a single episode of shortening, this requires pre-existing faults for localization of folding and thrusting. Furthermore, the thickness of Jurassic deposits differs in both limbs of the Karwendel and Thiersee synclines (Nagel et al., 1976) and the maximum sedimentary thickness of Upper Jurassic strata is located in the overstep area between the two synclines (Figure 1b). The strata present a clear facies differentiation and a generally increasing thickness of basinal Jurassic strata, from 100 m near Mittenwald (30 km W of the study area) to 1100 m in the Bächental (10 km NW of the study area; e.g., Ulrich, 1960; Nagel et al., 1976; Schütz, 1979; Ortner and Kilian, 2016; Gruber et al., 2022) (Figure 1b), showing an increased subsidence toward the SE end of the Karwendel syncline. This suggests that a basin existed that was bound by normal faults at a high angle to the faults in the synclines. Since major normal faults have not been mapped east of the Achental thrust, we interpret a W-dipping blind fault controlling deposition and facies differentiation in the Jurassic. Pliensbachian and Toarcian mass-flow sediments and scarp-breccias that are found near the basin slopes (Spieler and Brandner, 1989) support this hypothesis. Based on the aforementioned, it was proposed that this Jurassic basin-and-swell topography, in the form of a N–S to NE–SW striking pull-apart basin (Spieler and Brandner, 1989; Ortner and Gruber, 2011) or negative flower structure (Sausgruber, 1994b)

bordered by E–W striking sinistral strike-slip faults, forms the foundation of the present-day Achental structure. We therefore use this basin geometry as the basis for our analogue models.
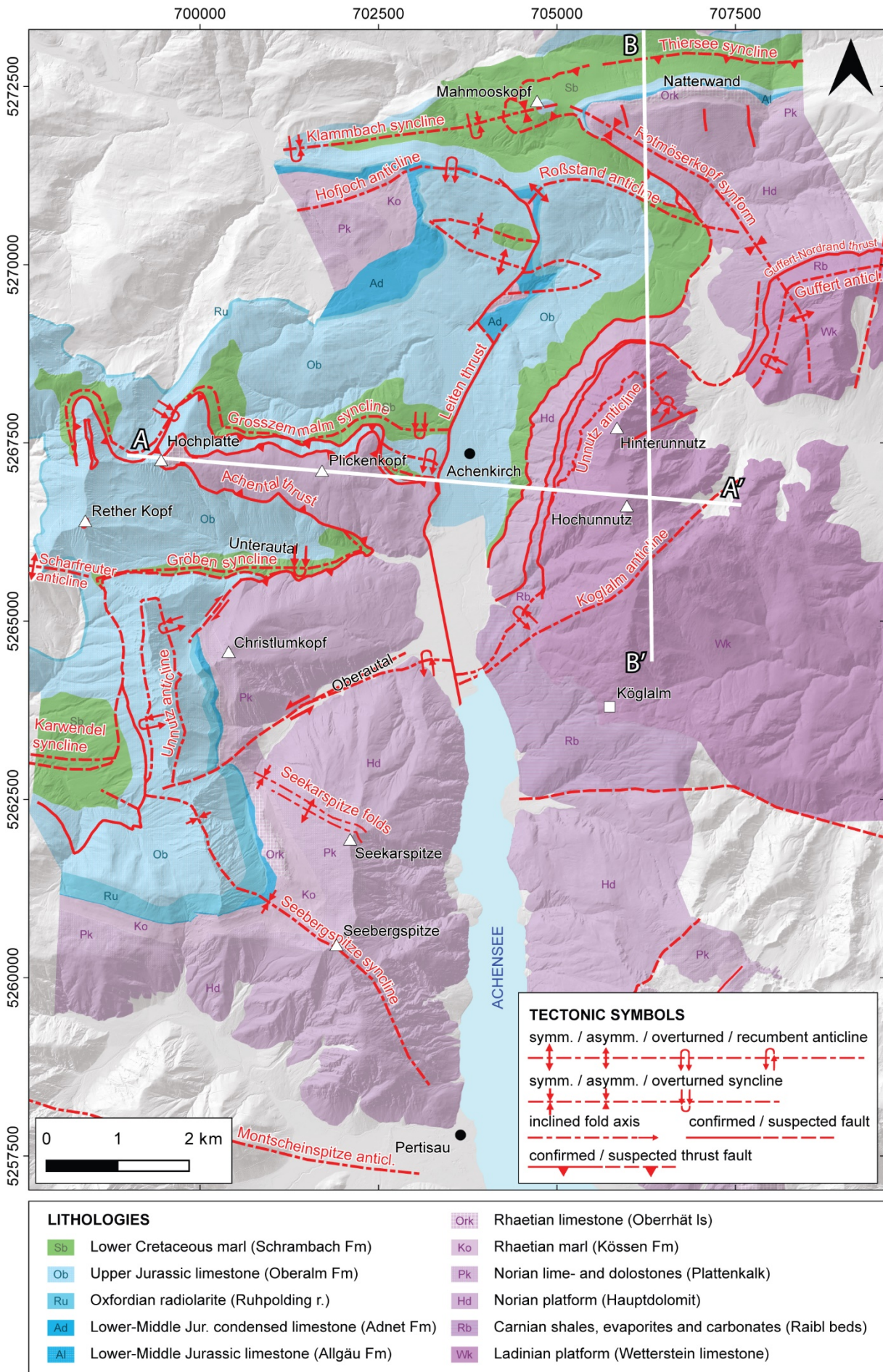
Figure 4: Geological map of the Achental structure compiled from Sausgruber (1994b), Spieler (1995), Auer (2001), Gruber (2011) and own data. Modified after Ortner and Gruber (2011). Sections A–A' and B–B' are shown in Fig. 5.
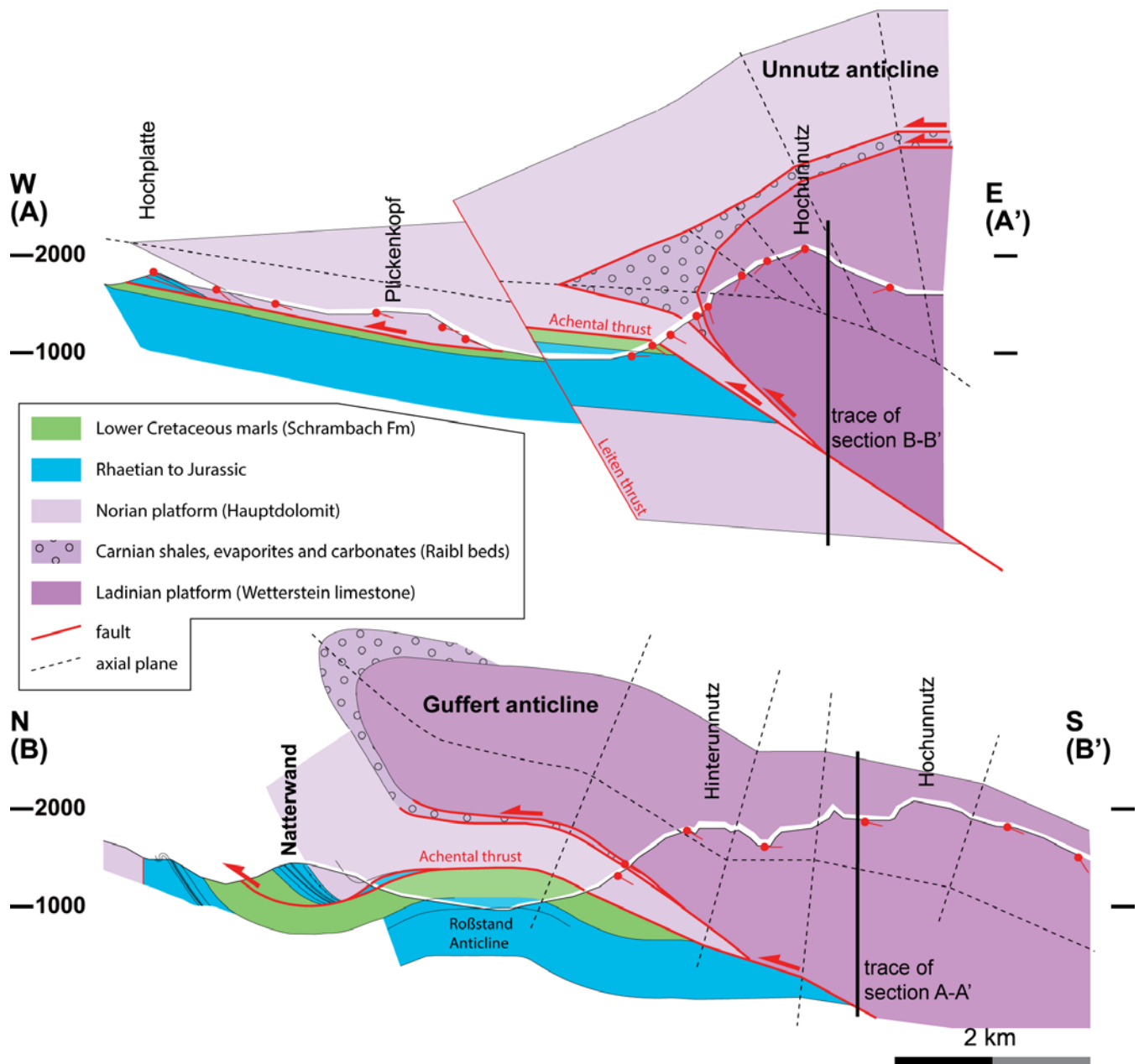
Figure 5: Cross sections (a) of the Unnutz anticline (Section A–A') and (b) of the Guffert anticline (Section B–B'). Section traces are marked in Fig.~~ure~~ 4. Modified after Ortner (2003b).

3 Analogue modelling

3.1 Modelling strategy

Regional-scale physical analogue modelling was conducted to investigate the influence of pre-existing basin-bounding extensional faults on oblique basin inversion, within the geological framework of the Achental structure. The goals of the experiments included testing 1) the importance of a weak basal décollement, 2) the influence of thick-skinned versus thin-skinned tectonics, and 3) the role of pre-existing structures in deformation localisation. Geological parameters from the natural example form the basis for our modelling approach. When translating geological structures into analogue models, a number of details and complexities are inevitably omitted, resulting in the creation of a simplified modelling basis that incorporates only the most important elements. In the case of the Achental structure, we have chosen to use the predicted Jurassic fault and basin geometry as a modelling basis, with a W-dipping normal fault and two E–W striking strike-slip faults. This is comparable to the basin geometry proposed by e.g., Ortner and Gruber (2011) and Spieler and Brandner (1989), and is based on facies and thickness changes within Jurassic deposits, as well as structural considerations outlined in Section 2.2. The rheological

properties of the NCA sedimentary succession, described in Section 2.1, were considered for the layering of the analogue models. For the basal Permotriassic Haselgebirge-Reichenhall succession we used ductile modelling materials (layer 1; Fig.~~ures~~ 3, 6). The middle and upper Triassic carbonate platforms are represented by brittle materials (layers 2 and 4). Rhaetian to Lower Cretaceous units are largely marls and marly limestones (Fig.~~ure~~ 3). Although these are considered less competent

265 units than the Ladinian and Norian platform carbonates, they are on the top of the analogue model and do therefore not control the modelling result. The Carnian Raibl beds were modelled using brittle or ductile materials, depending on the specific model (layer 3; Fig.~~ure~~ 6). Analogue models were set up to simulate the lithological and structural configuration of the eastern margin of the Jurassic Achental basin, resulting in an increasing model complexity.
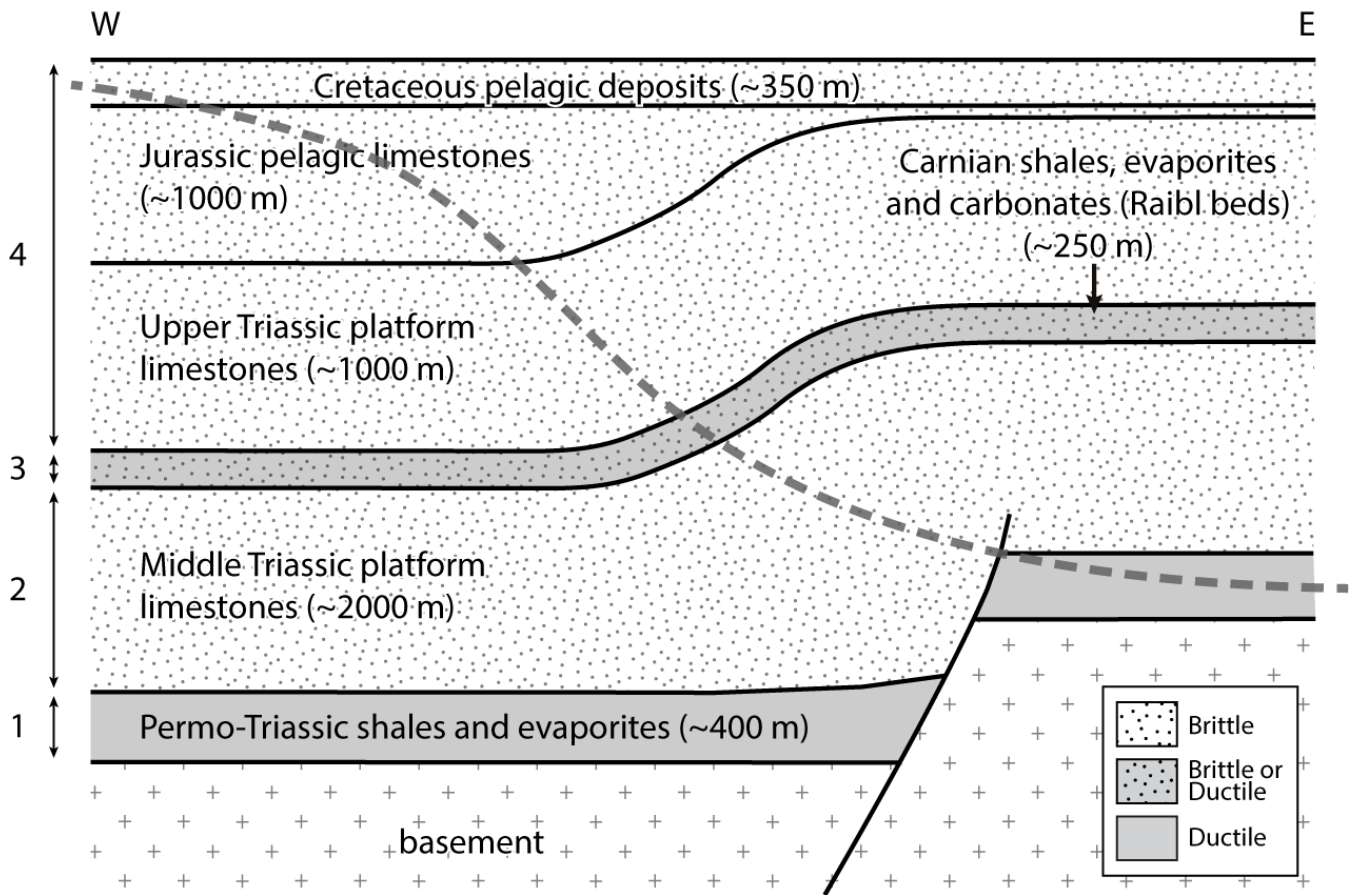
270 **Figure 6:** Schematic diagram showing the geological set-up of the eastern margin of the Achental basin, prior to inversion. Dashed line represents ~~inversional~~ trace of the Achental thrust. Lithologies are marked brittle or ductile, depending on their mechanical properties. Numbers refer to layers in Fig.~~ure~~ 3.

3.2 Modelling setup

Brittle and ductile modelling materials represent different parts of the NCA and Tethyan stratigraphy (Fig.~~ures~~ 3, 6). A ductile

275 layer of ~ 400 m thick, incompetent evaporites and shales, forming the basal décollement of the NCA was represented by silicone putty in models, with a thickness of 0.4 cm (Fig.~~ures~~ 6, 7a). The silicone putty is a mixture of RBG-0910 Dow Corning silicon polymer and iron powder (~ 32 wt.%) with a density of ~ 1360 kg m^{-3}. We determined a viscosity (η) of 20456 Pa s for the modified silicone putty, using a coni-cylindrical viscometer under room temperature (21 ± 1 °C) (Mooney and Ewart, 1934; Lee and Warren, 1940; see also Willingshofer et al., 2005). The viscosity of natural evaporites, albeit highly variable, is

280 estimated to be 10^{19} Pa s (Allen and Beaumont, 2016; Weijermars, 1986b, 1986c, 1986a; Weijermars et al., 1993; Weijermars and Schmeling, 1986), resulting in a viscosity scale-ratio of $2.046 \cdot 10^{-15}$. The silicone putty exhibits near-Newtonian behaviour and has an n-value of 1.27 in laboratory tests. The predominantly carbonatic, brittle sedimentary cover of the NCA was represented by dry quartz sand (Fig.~~ure~~ 6), a Mohr-Coulomb material, with a density of 1500 kg m^{-3} (e.g., Willingshofer et al., 2018). The quartz sand was sieved on top of the silicone putty, to create a total model thickness of 5 cm (Fig.~~ure~~ 7a). The

285 density of the natural prototype was approximated by the density of Triassic Muschelkalk, which is ~ 2680 kg m^{-3} (Manger, 1963: p. E31), resulting in a density ratio (ρ*) of 0.56 between model and nature. An intermediate layer of Upper Triassic carbonatic-evaporitic strata (Raibl beds) was modelled as either brittle or ductile layer, depending on the model-specific set-up (Fig.ure 7a.– b). For a discussion whether this unit behaves incompetent or not, see Kilian et al. (2021). Assuming that inertial forces can be neglected in the analogue models (see discussion in Wickham, 2007; Del Ventisette et al., 2007), the

290 scaling of time and length is allowed to deviate from the principle of dynamic similarity and their "ratios can be considered as independent variables" (Dombrádi et al., 2010: 109). The principles of dynamic, geometric and rheological scaling are discussed in Hubbert (1937), Ramberg (1981), Weijermars and Schmeling (1986), Merle and Abidi (1995), Brun (1999), Sokoutis et al. (2000; 2005) while their relationships between model and nature are summarized in Table 1.

295 ~~**Table 1:** Summary of model parameters. Experimental material parameters from Willingshofer et al. (2005; 2018). For strength envelops, see Figure 7b.~~

Materials/parameters		Model	Nature	Ratio (m/n)
Brittle layer	Thickness	Max. 0.05 m	Max. 5000 m	10^{-5}
(Quartz sand)	Density	1500 kg m^{-3}	2680 kg m^{-3}	0.56
	Strength	Max. 1471.5 Pa	Max. $2.63 \cdot 10^{-8}$ Pa	$5.597 \cdot 10^{-6}$
Ductile layer	Thickness	0.004 m	400 m	10^{-5}
(Silicone mixture)	Density	1360 kg m^{-3}	2450 kg m^{-3}	0.56
	Viscosity	20456 Pa s	10^{19} Pa s	$2.046 \cdot 10^{-15}$
	Strength	28.41 Pa	2550933 Pa	$1.11 \cdot 10^{-5}$
	n-value	1.27		
Length				10^{-5}
Convergence rate		$2.77778 \cdot 10^{-6}$ m/s	$1.02422628 \cdot 10^{-10}$ m/s	27137
Time		28800–39600 s	$7.8146208 \cdot 10^{-13}$– $1.0747469 \cdot 10^{-14}$ s	$3.685 \cdot 10^{-10}$
Bulk shortening		0.08–0.11 m	8000–11000 m	10^{-5}

Table 1: Summary of model parameters. Experimental material parameters from Willingshofer et al. (2005; 2018). For strength envelops, see Fig. 7b.

Model materials were placed in a rectangular fault box with metal bars as sidewalls and a wooden piston of 40 or 83 cm width

300 as a moving wall (Fig.ure 7c). We chose a length scale-ratio (L*) of 10^{-5}, so that 1 cm in the model represents 1 km in nature (Table 1). In all experiments, a pre-existing normal fault, similar to the boundary fault of the Achental basin was represented by a rigid basal plate (footwall block) with a 60° dipping ramp (fault plane). In model-specific set-ups, the direction of shortening (at 90 or 45° to the ramp), the movement of the basal plate (fixed or mobile) and the layering sequence of the model (Fig.ure 7a) were varied (Table 2). Shortening at 90° to the ramp represents the simplest possible scenario, whereas shortening

305 at 45° to the ramp reflects oblique shortening during Cretaceous shortening. Moving the basal plate with the brittle-ductile materials on top represents thick-skinned shortening, whereas a fixed basal plate with movement only in the brittle-ductile cover reflects thin-skinned shortening of the NCA. A varying layering with zero, one or two décollements tests the importance of a weak basal décollement and decoupling at the base or within the sedimentary cover.

The modelling strategy evolved from a basic brittle model (A) using the simplest geometric, kinematic and lithological parameters possible. The same model set-up was then applied to brittle-ductile (B1–B3) models. The set-up featured a basal plate with dimensions of 40 x 22.5 cm, a thickness of 1 cm and a 60° dipping front ramp (Fig.ure 7), representing the Jurassic normal fault. A wooden piston of 40 cm width was placed behind (A, B1) or on top of (B2, B3) the basal plate, so that the plate was either mobile or fixed, exemplifying the effect of thick- versus thin-skinned tectonics. Shortening was applied at 90° to the front ramp with a convergence rate of 8 cm/h for the brittle model (A) and 1 cm/h for the brittle-ductile models (B1– B3), and a total shortening of 8 cm (Table 1). The convergence rates between brittle and brittle-ductile models vary, because the strength of the ductile material depends on e.g., the strain rate, whereas this is not the case for brittle materials. For the brittle model, only quartz sand was used as a modelling material. In the brittle-ductile models, a basal layer of silicone putty was placed on top of the basal plate (B1, B3) or over the basal plate, ramp and table top (B2). For technical reasons model B1 (and, for comparison, model B3) do not have silicone putty on the table top, because the material may stick beneath a mobile basal plate, creating modelling artefacts. Model set-ups with a fixed basal plate do not have this problem. A small amount of dishwashing soap was spread between the plate and the silicone putty, to prevent sticking of the ductile layer to the substrate. Model B2 featured an additional, upper ductile layer (Fig.ure 7a), representing incompetent behaviour of the Carnian Raibl beds (Fig.ures 3, 6).

For model C we added two plates to the north and south of the main basal plate, to simulate E–W striking strike-slip faults and expected sigmoidal fault arrangement in the subsurface of the Achental structure. This required the use of a piston with a width of 83 cm. The basal plates were fixed, representing a thin-skinned style of deformation. Shortening remained orthogonal to the ramp at 1 cm/h, but total shortening was increased to 11 cm to accommodate the larger size of the model set-up. The basal ductile layer of silicone putty was placed on top of the basal plates and on the table top, but was disconnected at the ramp (Fig.ure 7) to create a clear velocity discontinuity as seen in model B3.

For models D1 and D2 the fixed main basal plate and two auxiliary plates were rotated 45°, to simulate Cretaceous oblique shortening at 45° to the ramp (Jurassic normal fault). We applied a total shortening of 11 cm, identical to model C. For both models, the basal ductile layer was placed on the basal plate and table top, while being disconnected at the ramp to create a velocity discontinuity as in model C (see e.g., Allemand and Brun, 1991; Tron and Brun, 1991). Model D2 featured an extra, upper ductile layer, simulating incompetent behaviour of the Raibl beds, similar to model B2.

Table 2: Summary of modelling runs and relevant parameters.

Series		Layering	Silicone		Basal plate	Plate border	Angle (°)	Total shortening (cm)
			# Layers	At ramp				
A		Brittle	0	---	Mobile	Straight	90	8
B	1	Brittle-ductile	1	Disconnected	Mobile	Straight	90	8
	2	Brittle-ductile	2	Connected	Fixed	Straight	90	8
	3	Brittle-ductile	1	Disconnected	Fixed	Straight	90	8
C		Brittle-ductile	1	Disconnected	Fixed	Sigmoidal	90	11
D	1	Brittle-ductile	1	Disconnected	Fixed	Sigmoidal	45	11
	2	Brittle-ductile	2	Disconnected	Fixed	Sigmoidal	45	11

Table 2: Summary of modelling runs and relevant parameters.
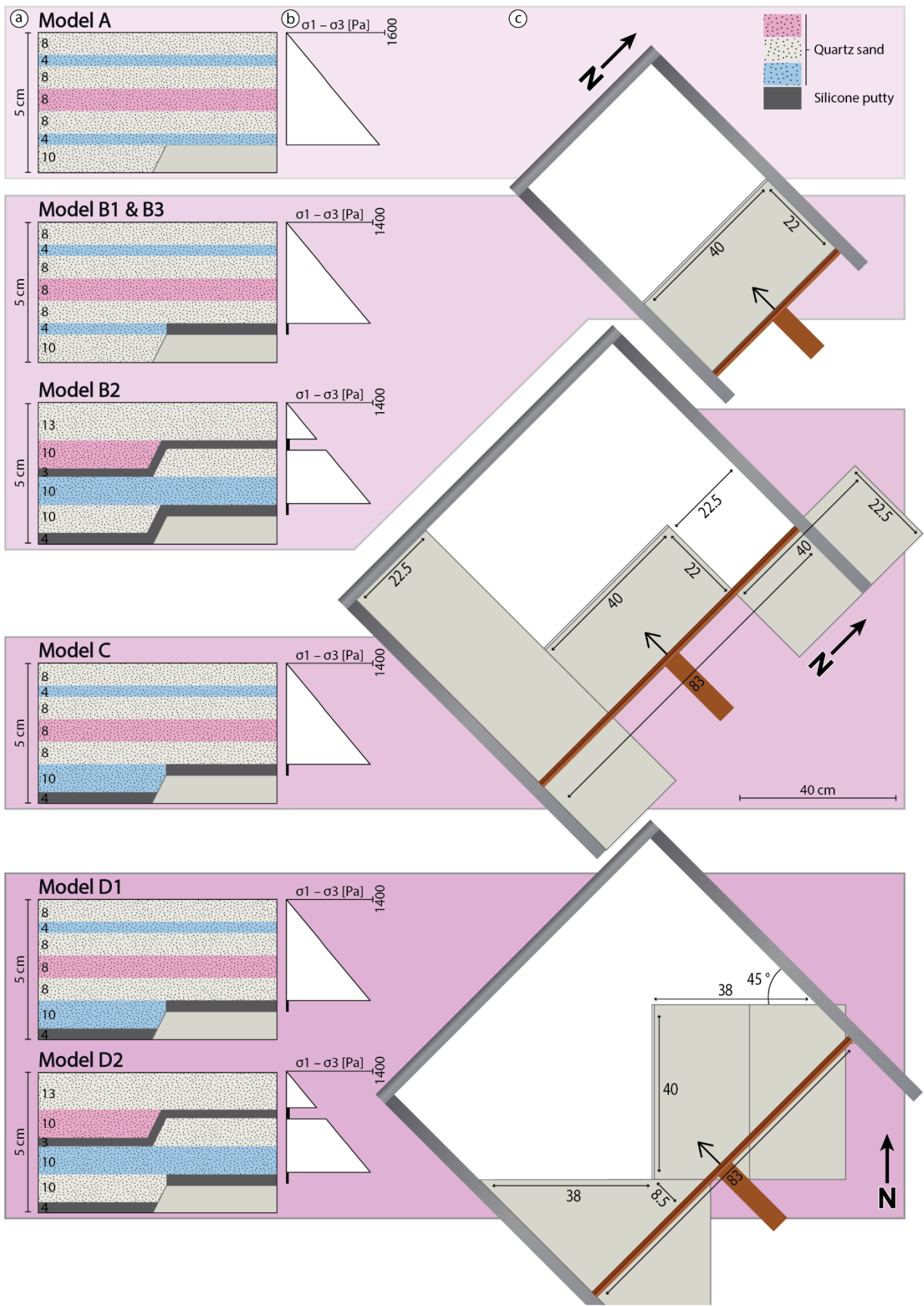
Figure 7: Modelling set-up for model series A–D. (a) Layering sequences show differently coloured layers of quartz sand and silicone putty with their respective thickness (in mm). The total thickness of the layering sequence was 5 cm. (b) Strength envelops show strength (in Pa) of different modelling materials. (c) Basal plate set-ups show the basal plate size (in cm).

3.3 Monitoring and model analysis

After reaching the desired shortening, models were covered with black sand for protection, drenched with water until saturation and left to rest for at least 2 hours. Sections were then cut orthogonal to the strike of major structures. Because these sections only show the final result and structure of the models, particle image velocimetry (PIV) was used to analyse incremental displacements in the analogue models (e.g., Leever et al., 2011; van Gelder et al., 2017), using powdered coffee grains on the model surface as markers. For all models, photographs of the top surface of the experiment were taken in a fixed time interval of 30 minutes. Photographs were then rectified to correct for lens distortion and processed using the MATLAB® vR2022a application PIVlab v2.57 (Thielicke and Sonntag, 2021; Thielicke and Stamhuis, 2014; Thielicke, 2014). In the image pre-processing settings, we enabled Contrast-Limited Adaptive Histogram Equalization (CLAHE) to locally enhance the contrast. FFT window deformation was used as the PIV algorithm. As post-processing steps we applied a velocity vector validation using a local median filter and interpolated missing data points.

The "strainmap" package (Broerse, 2021) for MATLAB® (vR2022a) was used for calculating cumulative strain type maps for models C and D1 based on incremental displacements from the PIV analyses. For a review of the underlying algorithms and practical applications of this software, see Broerse et al. (2021) and Krstekanić et al. (2021; 2022). Resulting colour-coded maps show the cumulative strain type (extension, strike-slip movement or shortening) at four points during the model runs (see figures in Section 4).

3.4 Limitations and simplifications

Similar to other analogue (and numerical) modelling studies, a measure of simplification is necessary to create a modelling basis from the natural example. Therefore, one of the major limitations of the experiments in this study is the necessary simplification of the initial fault configuration. The Jurassic basin-bounding faults are presently not exposed at the surface and thus their geometry and exact position are not known. It is assumed that the major present-day structural elements are aligned to the margins of the Jurassic Achental basin (Sausgruber, 1994b; Töchterle, 2005; Ortner and Gruber, 2011). Arguments for the existence of such a basin are presented in Section 2.2. Following the geometrical considerations for this basin, we chose a simplified subsurface fault arrangement with one N–S and two E–W striking elements as the basis for the final series (C, D) of analogue models. Splay faults and additional basin-bounding faults are thus not considered here. The models were shortened in one single phase, simulating Cretaceous NW-directed shortening. However, the Achental structure was affected also by N-directed Paleogene and NE-directed Neogene shortening (Eisbacher and Brandner, 1995; Ortner and Gruber, 2011). These posterior phases of deformation were not taken into consideration for the analogue modelling, because they cannot explain the large offset along the Achental thrust in W–E sections (Ortner and Gruber, 2011; Ortner, 2003b) and are therefore not expected to have created the main structural elements. The model set-up emphasizes the rheological contrast between a weak ductile basal décollement and a stronger upper brittle layer, whereas the characteristic, more complex heterogeneity of the NCA sedimentary cover was not included. Finally, the models ignore natural recovery processes such as erosion and sedimentation, which may influence the time-space evolution of structures. Eliminating limitations by increasing the complexity of models may increase the likeness between the analogue models and the natural example, but clouds the aim of analysing deformation localisation at pre-existing basin boundaries. Despite the simplifications described in this section, we are confident that our analogue model results are meaningful for the problem under consideration.

4 Results

Model A is a purely brittle experiment with a maximum thickness of the sand layer of 5 cm. The piston pushed both the sand and the basal plate. In the initial stages of the experiment, an asymmetrical pop-up structure with a master back-thrust (1) and

an antithetic fore-thrust (1) formed (Fig.ure 8). Further shortening was accommodated by transient fore-thrusts (2, 6–8), which developed at the base of the ramp and migrated upward through the wedge, along the master back-thrust.
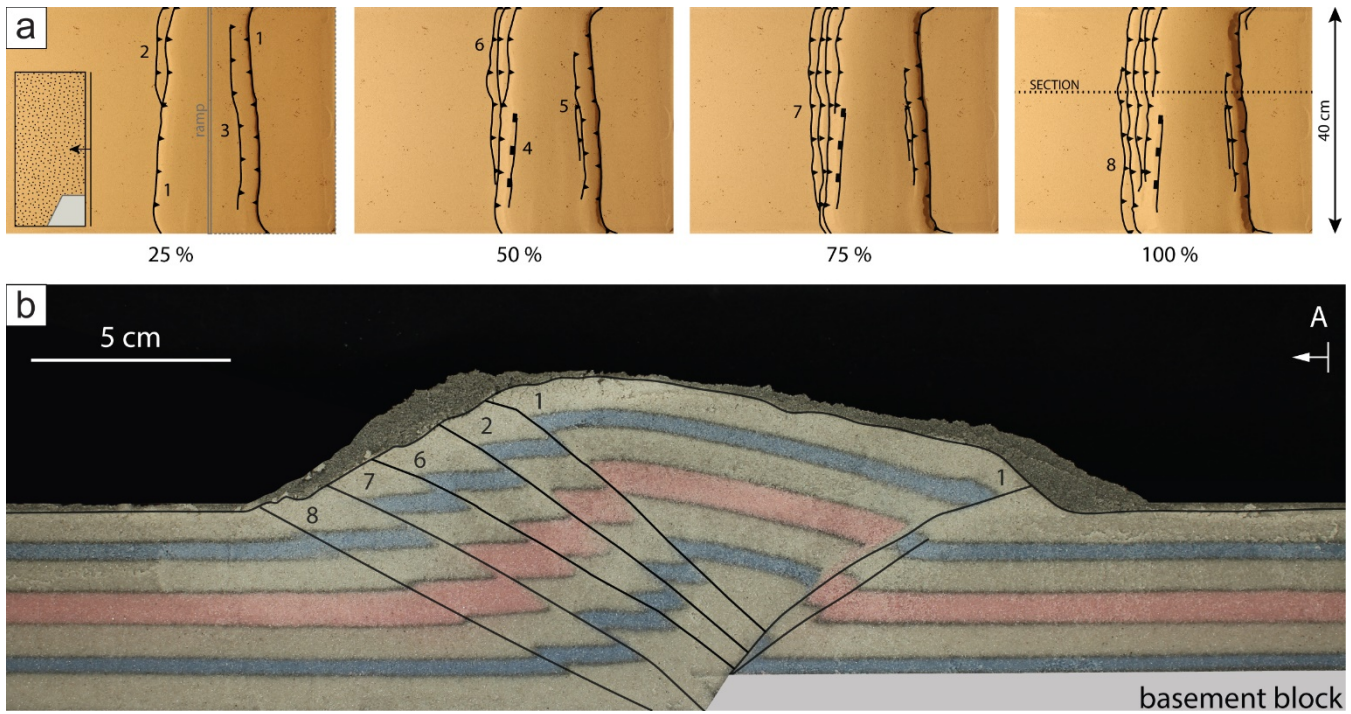
Figure 8: Modelling results of model A, showing (a) top views at 25, 50, 75 and 100 % of total shortening, and (b) side view at 100 % of total shortening. Location of section is marked in (a). Numbers show sequence of fault formation. The inset in the first top view photograph shows the modelling setup in cross-sectional view.

Model B1–B3 (Fig.ures 9, 10) are brittle-ductile models with a basal décollement of silicone putty, designed to study coupling and decoupling processes at the basal plate and ramp. Model B1 initially developed an asymmetric pop-up structure with an antithetic fore-thrust (1) and a master back-thrust (2) similar to model A (Fig.ures 9a, 10a). Although shortening was initially accommodated equally along the back-thrust and the fore-thrust, bulk shortening occurred along the master back-thrust. With further shortening, additional fore-thrusts (7, 9) form and former thrusts migrate upward along the master back-thrust. All major thrusts originate from the velocity discontinuity at the ramp. Several secondary pop-up structures formed along splay faults (e.g., 3, 4, 6). The final resulting wedge is both wider and lower than in the brittle model A, and the internal wedge structure more complicated. Model B2 contained an additional, upper ductile layer. Furthermore, the basal ductile layer was draped over the entire model base and connected at the mobile ramp (Fig.ure 7a). During the first 25% of total shortening, a central wedge developed over the ramp, formed by two main back-thrusts separated at the upper layer of silicone putty. At ~50% of total shortening hinterland deformation created an asymmetrical pop-up structure with a main back-thrust in the lower sand layers, and a symmetrical pop-up structure in the upper sand layer above the upper ductile horizon. Pockets filled with air, which was trapped underneath the silicone during model construction, represent modelling artefacts. Overall, the height of the resulting wedge was far less than in model B1 and structures were mainly hinterland-oriented and dominantly backwards thrusting (Fig.ures 9b, 10b). Thrusts may have initially originated at the velocity discontinuity, but were laterally transported onto the mobile basal plate as shortening progressed. The upper and lower sand layer were completely decoupled at the upper silicone layer. For model B3 we used a layering identical to model B1, but the basal plate was fixed to simulate thin-skinned deformation (Fig.ure 7). In the first half of the experiment (0–50% total shortening), a flip-type pop-up structure (see Smit et al., 2003: their Fig.ure 4) with two back-thrusts and conjugate fore-thrust (1) developed directly in front of the piston (Fig.ures 9c, 10c). Movement occurred along the main back-thrust, switched to the fore-thrust and back to the secondary back-thrust, as visible from lobes of silicone putty along the thrusts. At ~ 75% of total shortening, thrusting propagated into the foreland to form a strongly asymmetric pop-up structure with a master fore-thrust (5) and a minor back-thrust (6). The master thrust

originated directly at the velocity discontinuity above the ramp. Although in the fixed plate scenario, as opposed to the mobile plate scenario, deformation did not localise directly above the ramp but rather required a wedge in the hinterland, the wedge geometry is much more asymmetric with most of the shortening occurring along a low-angle master fore-thrust that is antithetic to the original normal fault geometry.
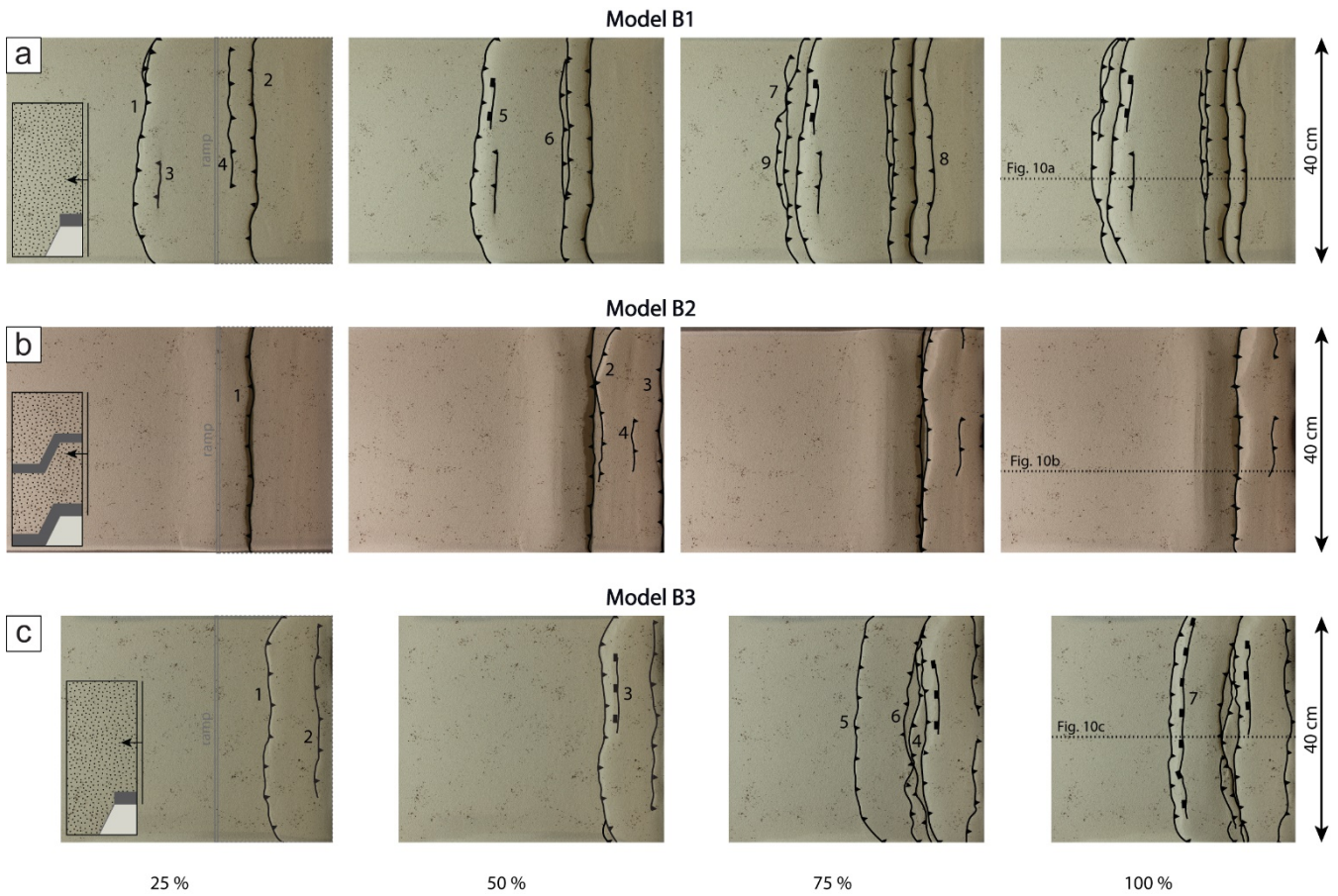
Figure 9: Top views of models (a) B1, (b) B2, and (c) B3 at 25, 50, 75 and 100 % of total shortening. Locations of sections are indicated (dotted lines). Numbers show sequence of fault formation. The insets in the first top view photographs show the modelling setups in cross-sectional view.
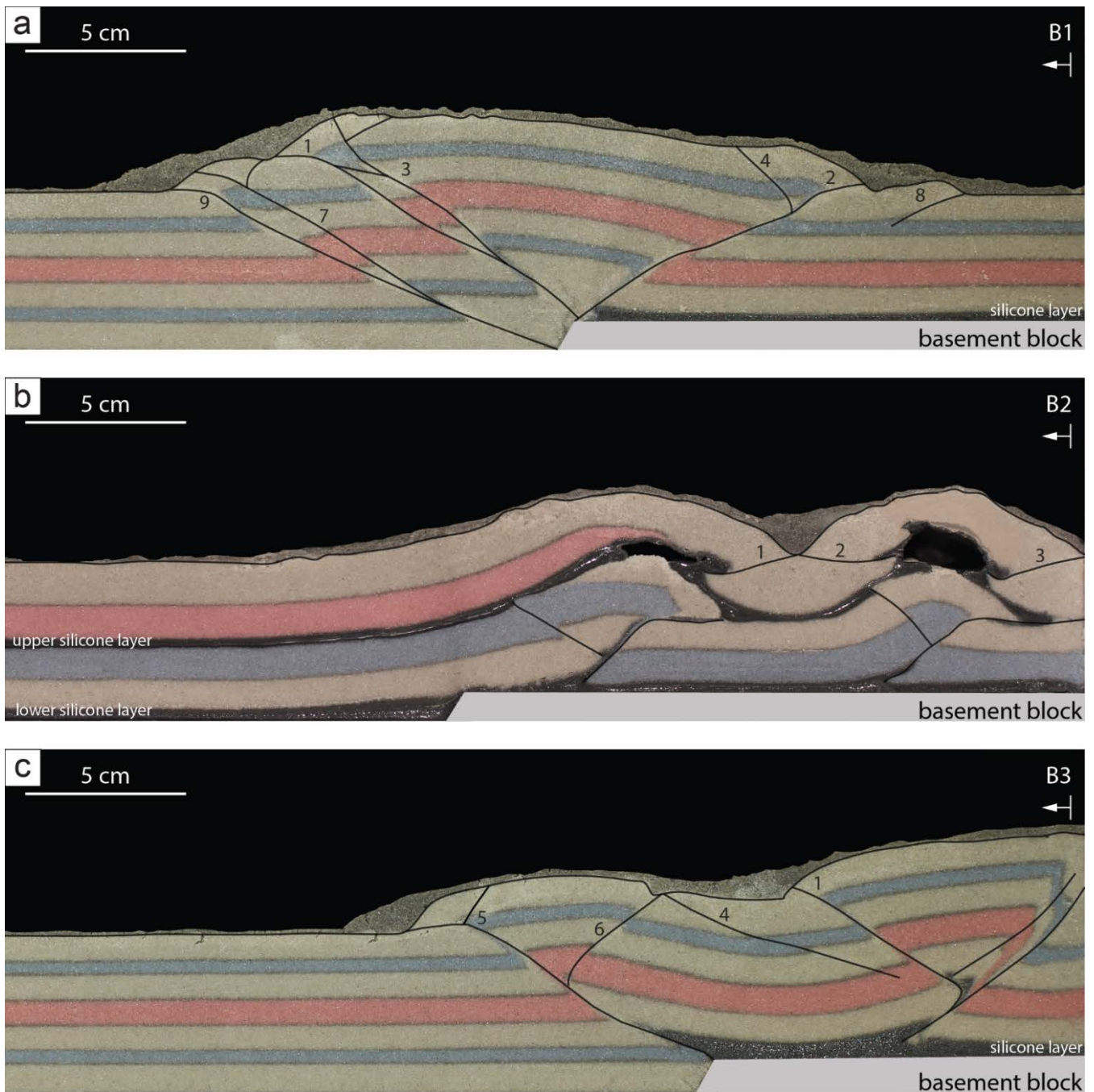
Figure 10: Side views of models (a) B1, (b) B2, and (c) B3 at 100 % of total shortening. Locations of sections are marked in Fig.~~ure~~ 9. Numbers show sequence of fault formation.

420 For model C, we used a basal plate geometry with three basal plates, aligned in an s-form (Fig.~~ure~~ 7c). We placed silicone putty on both the basal plates and the table top, disconnecting it at the ramp to form a similar mechanical scenario as in model B3. Initially, a slightly asymmetrical pop-up structure formed close to the piston, with a back-thrust that migrated slightly upward along the main fore-thrust (2) (Fig.~~ure~~ 11a,~–b). Additional fore-thrusts (1, 3) developed especially in the northern area of the model, where the basal plate was missing. After ~ 55% of total shortening, deformation propagated into the foreland,

425 where a second asymmetric pop-up structure formed above and parallel to the ramp in the subsurface. The master fore-thrust (5) accommodated most of the shortening, whereas several minor back-thrusts migrated upward along the master thrust. The sand layer forms a ramp anticline over the master thrust, which approaches lower angles toward the surface. Close to reaching the total shortening, deformation propagated in the southern area of the model, where the basal plate reaches into the foreland, and third pop-up structure was formed there (9), but was not able to develop further with this amount of shortening. Overall,

430 the wedge was relatively low compared to the brittle model A and the brittle-ductile model B1. The deformation front at total shortening approximately shows the contours of the basal plate in the centre and southern parts of the model (Fig. 11a).

PIV analysis of (surficial) shortening shows that deformation occurs in the tectonically active region west of the deformation front, with strain localisation at the foremost thrust (2, 5, 9/10). Strain directions rotate outward on both the northern and southern side of the wedge. The dominant type of strain at the active fore-thrusts is shortening (red colours in Fig. 11c).
435 Extensional strain on top of the wedge (blue colours in Fig. 11c) is mainly caused by gravitational collapse of parts of the wedge. We attribute local strike-slip strain (indicated by yellow to turquoise colours in Fig. 11c) to erroneous vectors generated by the PIV analysis in areas where individual sand grains could not be tracked optically.
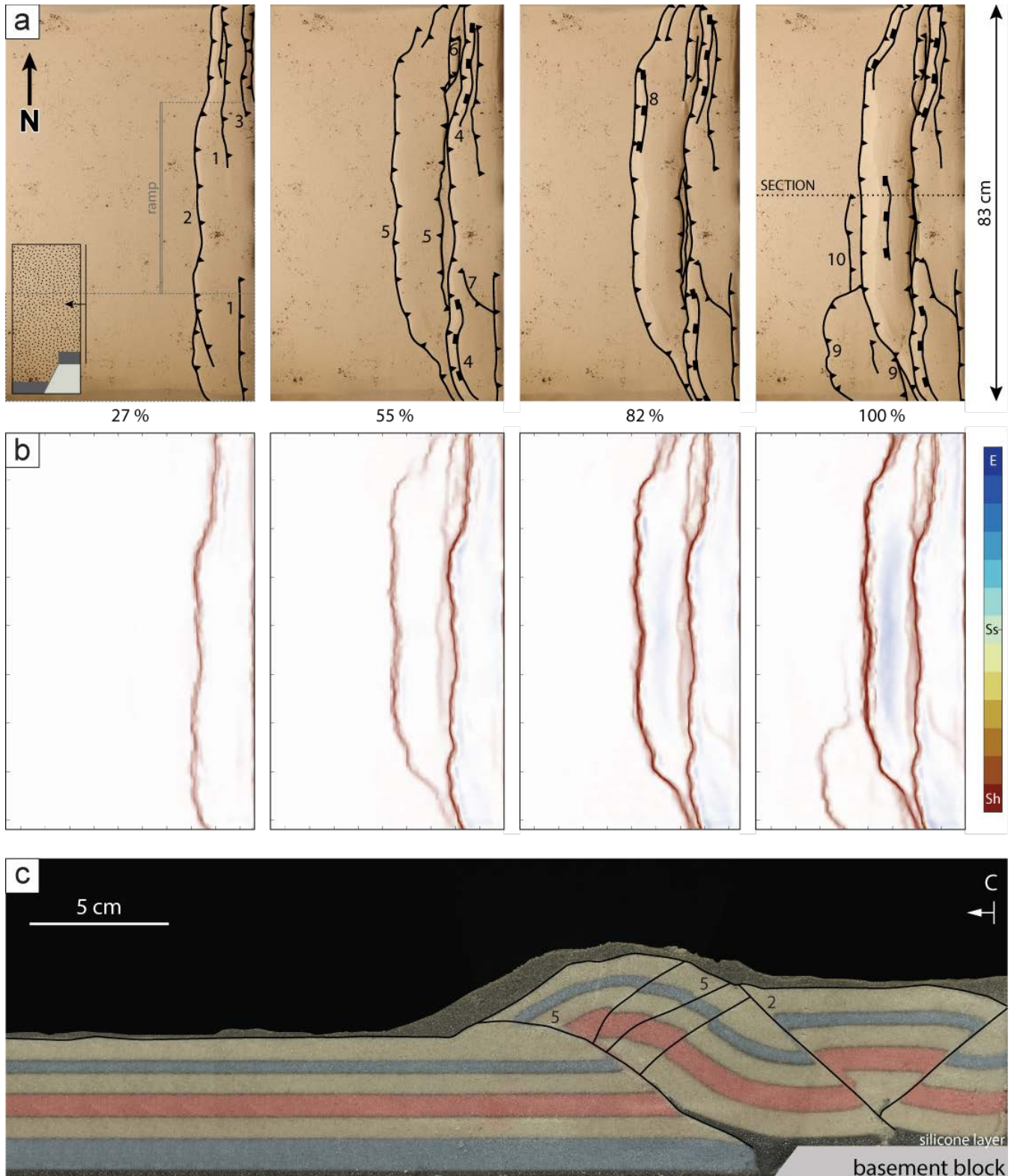
For model D1 and D2 shortening was directed at an angle of 45° to the basal plate and ramp (Fig.~~ure~~ 7c). Model C and D1 used an identical layering sequence. In the initial stages of the experiment (< 55% total shortening), a pop-up structure developed over the entire length of the piston (Fig.~~ure~~ 12a). This structure is asymmetric with a main fore-thrust in the south. In the central area of the model, where the basal plate set-up creates a 90° angle, the structure is of a flip-type (see Smit et al., 2003: their Fig.~~ure~~ 4), where shortening was initially accommodated along a fore-thrust, before switching to a back-thrust. From approximately 27% of total shortening on, the wedge widened along the main fore-thrust (1) in the south, where the basal plate extends into the foreland, whereas in the centre and north of the model, shortening was accommodated by a series of fore-thrusts (3–5) that migrated along an associated back-thrust. From ~ 82% of total shortening, the wedge propagated on the southern basal plate (7), and then on top of the northern plate (8). The surface expression of the propagating fore-thrusts runs parallel to the plate structure in the subsurface. The thrusts originate directly at the velocity discontinuity at the ramp (Fig.~~ure~~ 13a,~~–~~ b) and form low-angle (~30°) master thrusts in strongly asymmetric pop-up structures, similar to model B3. At the 90° corner between basal plates a steepening of the back thrust and migration of irregularly spaced fore-thrusts within the pop-up structure accommodate shortening.

PIV analysis of incremental displacements shows that shortening localises at the foremost thrust in model D1 (1, 7). The strain type patterns are similar to model C, with shortening as the dominant strain type, and the dominant strain direction perpendicular to the thrust trace. The orientation of the basal plates in the subsurface evidently controls the orientation of the thrusts, with a local rotation of the strain field.

Model D2 used the same basal plate set-up as model D1, with a layering sequence using two ductile layers, similar to model B2 (Fig.~~ure~~ 7). Similar to model B2, the upper and lower part of the model are decoupled at the upper ductile layer. Propagation into the foreland occurred at ~ 55% of total shortening. In the lower part of the model, pop-up structures with a master fore-thrust localised at the ramp (Fig.~~ures~~ 12c, 13c). These structures form a sigmoidal shape that straddles the basal plate structure in the subsurface. The decoupling at the upper ductile layer caused that the surface structures differ from the lower part of the model and the wedge reached far less height than in experiments with a single ductile layer.
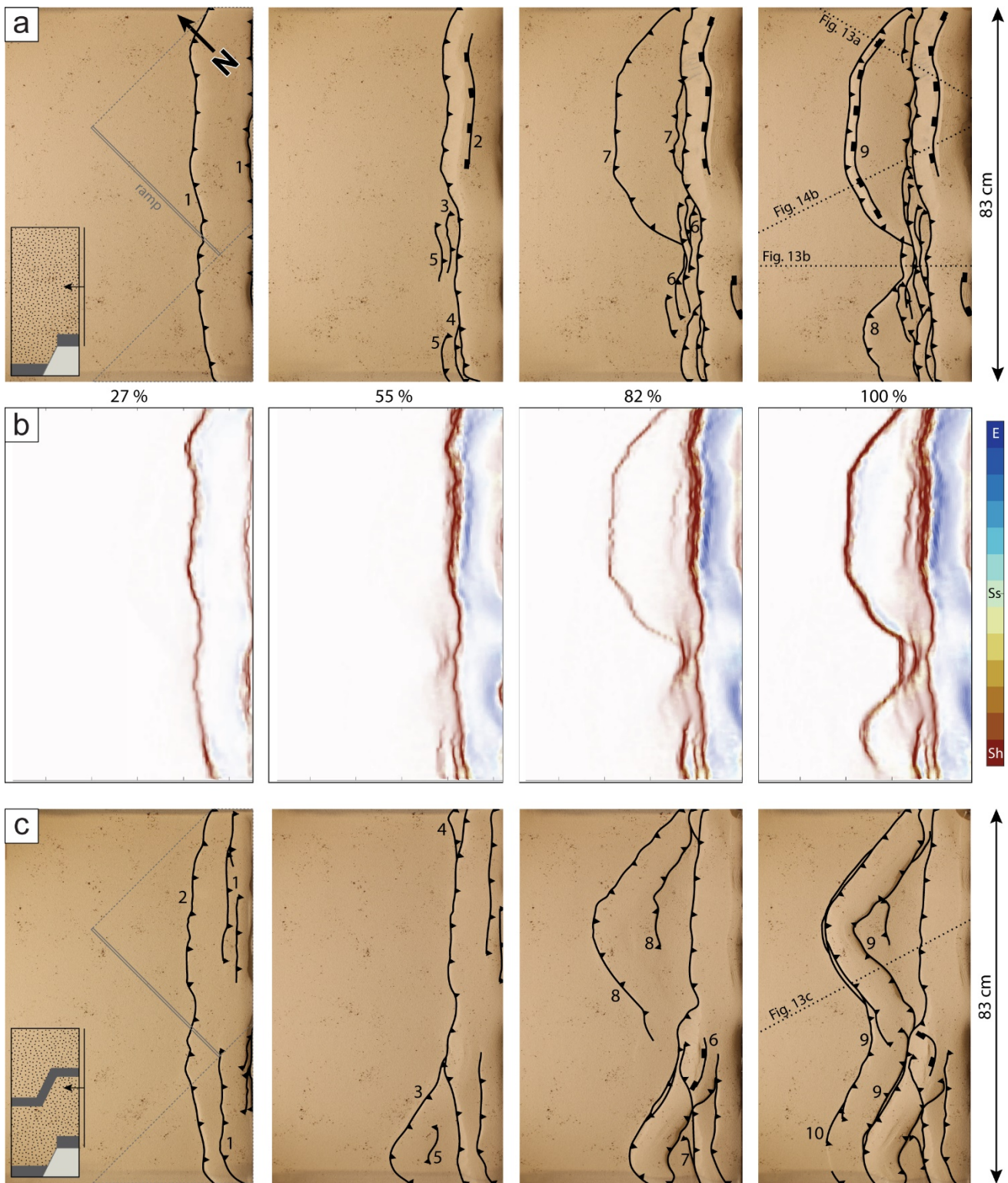
Figure 12: Top views of models (a) D1, and (c) D2 at 27, 55, 82 and 100 % of total shortening. Numbers show sequence of fault formation. The insets in the first top view photographs show the modelling setups in cross-sectional view. PIV strain type analysis of model (b) D1, showing areas of extension (E), strike-slip movement (Ss) and shortening (Sh).
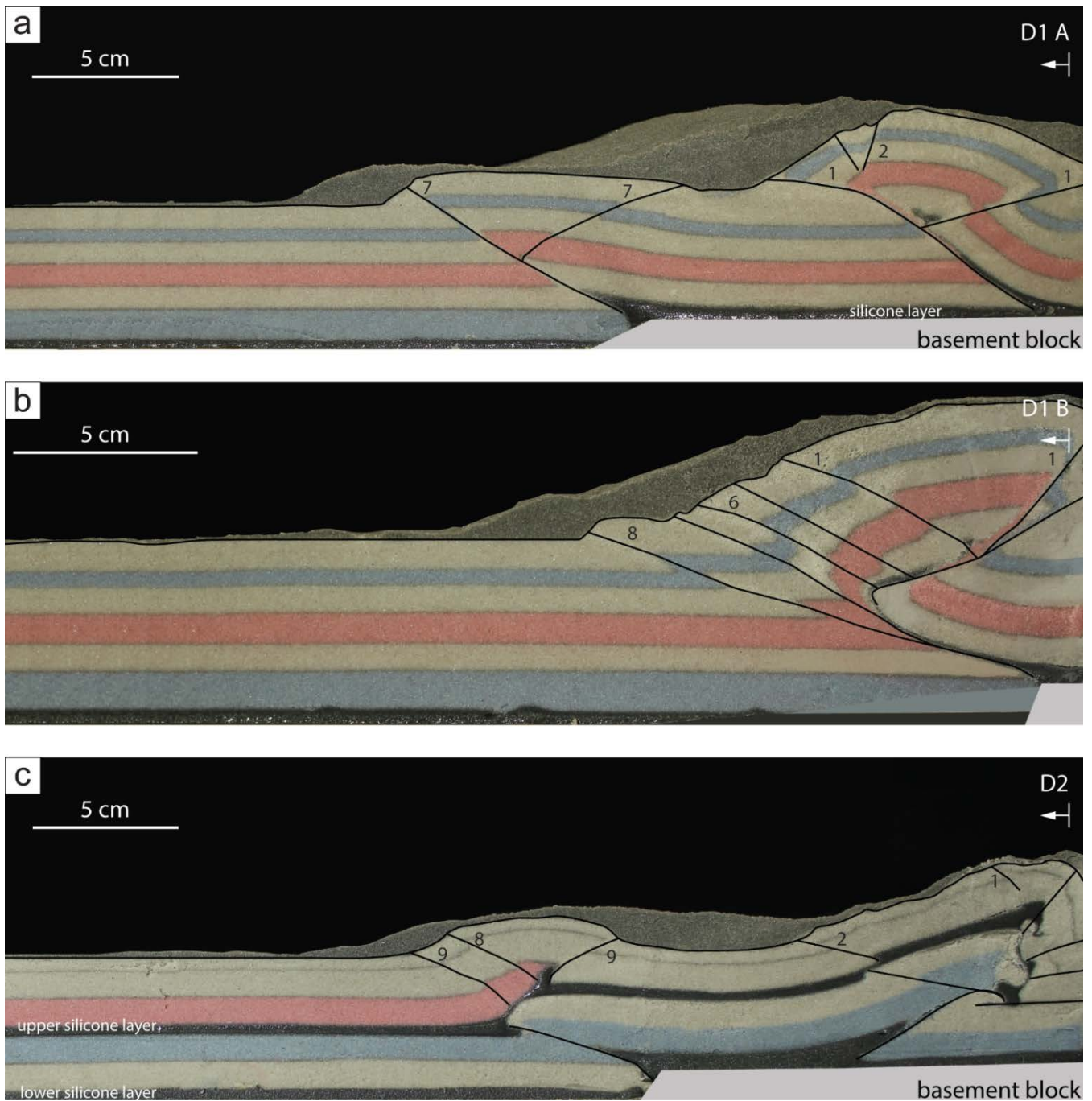
Figure 13: Side views of models (a, b) D1, and (c) D2 at 100 % of total shortening. Numbers show sequence of fault formation.

5 Discussion

5.1 Analogue modelling

475 Inversion of basins, whether orthogonal or oblique to the former basin margins, has been subject of many analogue modelling studies (e.g., Deng et al., 2020; Yagupsky et al., 2008; Del Ventisette et al., 2006; Bonini et al., 2012; Brun and Nalpas, 1996; Zwaan et al., 2022; Molnar and Buiter, 2023; Sieberer et al., 2023). The high variance of geological structures leads to a myriad of deformation styles characterizing inverted and reactivated fault systems (Bonini et al., 2012: their Fig.~~ure~~ 3), especially for inversion set-ups involving a viscous décollement (Brun and Nalpas, 1996). The modelling strategy (see Section 3.1) followed

480 in this study aimed to test factors that may affect the structural grain of obliquely inverted extensional basins, including the influence of 1) a weak basal décollement, and 2) pre-existing structures attributed to an extensional basin. The increasing complexity of the models is a result of consecutively implementing parameters that were found to be of relevance to the natural

example, the Achental structure. Apart from its sigmoidal hanging wall shape, one of the complexities of the Achental structure is that its dominant fore-thrust is antithetic to the Jurassic normal fault in the subsurface (Fig. 6). Most of the structures

485 associated with basin inversion are synthetic to existing normal faults (e.g., Héja et al., 2022: their Fig. 4 and 11; Bonini et al., 2012: their Fig. 3), although the formation of an antithetic low-angle thrust has been described (Laubscher, 1986; Tavarnelli, 1996) and simulated in the context of thin-skinned deformation of the Jura fold and thrust belt (Caër et al., 2018).

5.1.1 Influence of mechanical stratigraphy

In our study, the influence of a weak basal décollement has been tested using two models (A and B1). These have an identical

490 mechanical set-up, using a rigid ramp, which represents a pre-existing normal-fault controlled mechanical heterogeneity in the model and is pushed into a brittle (A) or brittle-ductile (B1) cover. The brittle-ductile model (B1) shows a narrower cross-sectional taper, a markedly lower angle of thrusting, wider thrust spacing and faster propagation compared to the brittle model (A). Decoupled thrust wedges are known to show these effects in nature (Jaumé and Lillie, 1988) and analogue models, attributed to a lower basal friction compared to frictional Coulomb wedges (Smit, 2005; Smit et al., 2003; Mulugeta, 1988;

495 Cotton and Koyi, 2000; Davis and Engelder, 1985). Thus, our brittle-ductile model B1 is able to better represent the low-angle character of the natural example than model A.

Models of oblique basin inversion show that the use of a ductile layer results in decoupling of the sedimentary cover and a strong localisation of deformation at existing extensional structures (e.g., Del Ventisette et al., 2006; Brun and Nalpas, 1996). Similarly, the use of an upper (second) ductile layer (models B2, D2) leads to a decoupling between the upper and lower

500 sediment cover (e.g., Fan et al., 2020; Del Ventisette et al., 2006). As a result, structures within the lower brittle layer are terminated at the upper ductile layer. Low-angle hinterland-dipping thrusts emerging from the velocity discontinuity are therefore not visible in top view (see e.g., model D2, Fig. 13). Decoupling thus prevents the formation of large-scale structures across the entire sedimentary cover.

5.1.2 Favourable kinematic conditions for basin inversion

505 The build-up of a certain height of the initial wedge at the backstop is a prerequisite for fault propagation, consistent with the critical taper theory of Davis et al. (1983) (see also Graveleau et al., 2012, and references therein). In all experiments, a wedge of 5.7–7.6 cm high was formed in front of the piston and at least 6 cm of shortening was needed for the thrusts to propagate into the foreland. The movement of the basal plate (i.e., fixed or mobile, simulating thin- or thick-skinned deformation) then greatly influences the structure and location of the resulting wedge in brittle-ductile models (compare e.g., model B1 and B3).

510 By using a mobile plate (model B1), this rigid block acts as a buttress, localising early deformation at the ramp and restraining further movement of thrust sheets (Bailey et al., 2002; Héja et al., 2022; Gomes et al., 2010). Further shortening was accommodated along a main back-thrust with multiple fore-thrusts, showing strong similarities to existing analogue experiments (e.g., Bonini et al., 2000; Persson and Sokoutis, 2002). The use of a fixed plate (model B3) leads to initial strain localisation at the backstop (see also Deng et al., 2020; Yagupsky et al., 2008; Caër et al., 2018). The mechanical contrast

515 between the rigid ramp, quartz sand and silicone putty forms a velocity discontinuity (Allemand and Brun, 1991; Tron and Brun, 1991), which is crucial for secondary strain localisation. The step at the ramp, where silicone putty and quartz sand meet, thus works as a "fault generator" or a "nucleation site for thrust faulting" (Yagupsky et al., 2008: 852), not dissimilar to the "thrust mill" of Laubscher (1986), which is also demonstrated in models that use silicone putty or glass microbeads as a weak layer (Yagupsky et al., 2008; Caër et al., 2018). At the same time, structures localising at the ramp accommodate a large

520 amount of shortening, preventing deformation from propagating further (Laubscher, 1986; Tavarnelli, 1996; Caër et al., 2018). A low-angle fore-thrust nucleating at the velocity discontinuity thus may accommodate a great amount of shortening.

5.1.3 Influence of structural inheritance

Propagation of deformation and strain localisation in brittle-ductile models led to the formation of structures oriented parallel to the basal plate boundaries in the subsurface. Other studies of oblique shortening of pre-existing grabens or steps show similar results, where newly formed reverse and thrust faults more or less outline the structure in the subsurface (e.g., Deng et al., 2020; Yagupsky et al., 2008; Caër et al., 2018; Molnar and Buiter, 2023). Whereas thrusts in models of Caër et al. (2018) appear to consistently dip towards the backstop, our PIV analyses show that the dominant strain direction is approximately perpendicular to the thrust trace, which can be explained by strain partitioning mechanisms. At the same time, the localisation of structures at steps and the geometry of the resulting low-angle fore-thrust with a hanging wall anticline (e.g., model D1, Fig. 13a, b) is similar to the models of Caër et al. (2018: their Fig. 4.11b–e) and it is evident that in models with oblique shortening (model D1, D2) thrust faults outline the basal plate structure.

The obliquity angle between the basin axis and subsequent shortening greatly influences structures formed by basin inversion (Brun and Nalpas, 1996; Yagupsky et al., 2008; Del Ventisette et al., 2006; Deng et al., 2020). In brittle experiments, low obliquity angles are associated with an increasing angle of the reverse faults (Brun and Nalpas, 1996) and dominant fore-thrusts, whereas a higher obliquity angle preferably creates symmetrical pop-up structures (Deng et al., 2020). Our brittle-ductile models were able to create a dominant fore-thrust that localizes at the ramp regardless of the obliquity angle (90° for models B–C, 45° for models D). However, fault localisation at subsurface steps was most distinctive in models with a lower obliquity angle (45°, models D). Our large-scale models (C and D) furthermore agree with those of Yagupsky et al. (2008) and Molnar and Buiter (2023), where the graben segment closest to the deformation front is reactivated first.

The analogue models (in particular models B3, C, D1; Fig. 9c, 10b, 12a) show that low-angle hinterland-dipping thrusts can originate at a pre-existing high-angle normal fault with an opposite dip (see also Fig. 6), as predicted (Tavarnelli, 1996; Laubscher, 1986). The pre-existing subsurface fault network is able to control the geometry of inversion structures. The models exemplify that through strain localisation at subsurface steps, the sigmoidal geometry of the Achental thrust hanging wall (see model series D, Fig. 12) can be created within a single deformation phase of oblique shortening.

5.2 Comparison with the natural example

In analogue models we aim to create a scaled and simplified version of the natural example, the Achental structure. We show that it is possible to form a sigmoidal structure, characterized by a low-angle main fore-thrust, hanging wall anticlines and a localisation at a pre-existing step, within a single phase of shortening (Fig. 14). Model parameters that were found to be applicable to the Achental structure are 1) a weak basal décollement, 2) thin-skinned deformation, and 3) a clear velocity discontinuity acting as a "fault generator". However, laboratory experiments cannot fully encompass the complexities of natural geological structures. In this section, we compare features of the analogue models and the Achental structure.

5.2.1 Mechanical stratigraphy

Rheological heterogeneity of sedimentary successions is an important parameter for both analogue models and natural processes. A brittle-ductile succession is able to re-create large-scale structures in analogue models. However, small-scale faulting and folding within the sedimentary cover of the NCA is cannot be reproduced by the analogue models (see also Fig. 14b). Comparison between brittle and brittle-ductile models shows that a very weak décollement is imperative for the low-angle Achental thrust to form at a pre-existing basement step. Whether or not this décollement is present in the hanging wall of the original normal fault, does not influence strain localisation in the models, although it might impact fault propagation with further shortening (Caër et al., 2018). An offset of the décollement, as opposed to a monocline across the ramp (model B2), increases the effect of the velocity discontinuity, but is not strictly necessary for localisation to occur. The Haselgebirge-Reichenhall succession at the base of the Karwendel thrust sheet forms the main décollement of the NCA (Eisbacher and

Brandner, 1995). An intermediate succession of Carnian shales, evaporites and carbonates (Raibl Fm) may also be represented by a ductile layer, decoupling the lower and upper carbonate platform. Kilian et al. (2021) argue that in this part of the NCA, the Carnian units mostly consist of carbonates (e.g., Jerz, 1966; Brandner and Poleschinski, 1986), which we modelled as competent units. Our analogue models with two detachment horizons show a complete decoupling between the upper and lower brittle section. Although in the Achental structure, small-scale folding dies out near the Hauptdolomit-Plattenkalk transition, the overall geometry of the Unnutz anticline is preserved through the entire outcropping sedimentary succession. Therefore, we dismiss the hypothesis that the Raibl Fm behaves as a significant decoupling horizon.

Carbonate units within the Achental structure are represented by quartz sand in analogue models, simulating brittle behaviour. This modelling material is not able to simulate folding of the Guffert-Unnutz-Montscheinspitze anticline. Resulting from the chosen modelling materials and scaling, important features of the natural example, e.g., the large overturned panels seen in the cross-sections (Fig. 5 and 14), cannot be explained by the analogue models. However, the thinning of strata in the hanging wall, close to the fault, could be reproduced (Fig. 14b). Ortner (2003b) proposes a progressive rollover-fault-propagation model (Storti and Salvini, 1996) for the Unnutz anticline. This type of folding leads to strongly overturned or recumbent anticlines in fold-and-thrust belts (Storti and Salvini, 1996) and involves a fault-propagation fold with strong, layer-parallel shear (flexural slip). Although for fault-propagation folds "important field evidence […] is the observation that some faults, particularly thrust faults, die out in the cores of folds." (Suppe, 1985: 350), this is not necessarily the case for progressive rollover-fault-propagation folds, because the overturned limb of the hanging wall anticline has been completely detached from the footwall (Storti and Salvini, 1996: their Fig. 2). Flexural slip accommodating deformation within the Guffert-Unnutz-Montscheinspitze anticline is seen from layer-parallel and very low-angle fault planes within Hauptdolomit, and support the progressive rollover-fault-propagation model. Fault-propagation folding as a mechanism is seen in the La Roche d'Or anticline, Swiss Alps (Caër et al., 2018), which formed along a thrust fault originating at a basement. Similar to the Reichenhall-Haselgebirge succession in the NCA, evaporitic sediments form a décollement between the basement and the sediment cover. Martin and Mercier (1996) provide a natural example of the western Jura, showing the development of a low-angle ramp above pre-existing structures of the Bresse graben. While the progressive rollover-fault-propagation model produces overturned panels, it does not explain e.g., the hinge collapse interpreted for the Unnutz anticline (Fig. 5a). Although thinning of the overturned limb is expected and can be seen in the analogue models as well (Fig. 14b), the complete elimination of stratigraphy in the overturned flank of the anticline cannot be explained by this type of folding.

In salt-detached fold-and-thrust belts the structural style is, among others, dependent on the amount of salt available (Hudec and Jackson, 2007; Lacombe et al., 2019). Within salt-controlled belts, anticlines are mostly (faulted) detachment folds, which can be mistaken as fault-propagation folds due to their superficial resemblance (Mitra, 2002). Detachment folding (e.g., Homza and Wallace, 1995; Josep Poblet, 1996; Epard and Groshong, 1995) and subsequent truncation and displacement of these folds (e.g., Suppe and Medwedeff, 1990; Morley, 1994; Jamison, 1987) produces asymmetric anticlines with steep to overturned forelimbs (Wallace and Homza, 2004). In the case of salt-related structures (e.g., minibasins), shortening will initially concentrate on these structures (Snidero et al., 2019; Duffy et al., 2018). Reactivation of salt welds as thrusts and rotation of flaps may produce overturned panels with incomplete stratigraphy (Granado et al., 2019; Granado et al., 2021; Rowan and Vendeville, 2006; Duffy et al., 2018). The exact type of deformation strongly depends on the original thickness of the Haselgebirge-Reichenhall succession. In the case of the Achental structure is it unknown how much salt was present originally. If a substantial amount was available, it might have controlled the geometry of overlying younger deposits. However, no major growth wedges or angular unconformities have been observed in the area up to now.

5.2.2 Kinematic parameters and structural inheritance

In analogue models, the use of a fixed basal plate translates to a thin-skinned tectonic style, in which the sedimentary cover is decoupled from the basement by a décollement (Rodgers, 1949). Such thin-skinned structural style is well known from the NCA (e.g., Eisbacher et al., 1990; Auer and Eisbacher, 2003). For localisation and propagation of deformation, the presence of a step in the subsurface and topography in the hinterland is important as well. The advancing front of the NCA fold-and-thrust belt and the uplift resulting from movement along e.g., the Eben thrust (Eisbacher and Brandner, 1996) (Fig. 1b) may have provided this topography. The Jurassic basin architecture in the subsurface is thought to have provided steps where deformation could localise (Fig. 14a). Facies differentiations of Jurassic sediments, a maximum thickness of Upper Jurassic sediments in the overstep area between the Karwendel and Thiersee synclines (Fig. 1c) (Schütz, 1979; Nagel et al., 1976), and documented Cretaceous transport directions oblique to the synclines (Sausgruber, 1994a, 1994b; Ortner and Gruber, 2011) underline the presence of such a basin (see Section 2.2). We assume that, corresponding to the geometry of the Achental structure, at least one N–S striking, west-dipping normal fault and two E–W trending strike-slip faults must have existed (Fig. 14a). Such a basin geometry is similar to Jurassic fault systems in more western parts of the Alpine orogen (Eberli, 1987, 1985; Weissert and Bernoulli, 1985) and has been proposed for the Achensee region (Eisbacher and Brandner, 1995, 1996; Channell et al., 1990).

The models were subjected to a single phase of oblique shortening, simulating NW-directed Cretaceous convergence related to Alpine orogeny. Field data from the Achensee area (Sausgruber, 1994b; Beer, 2003) support NW-directed shortening. Ortner and Gruber (2011) argue that the offset in the central Achental thrust is larger than in its northern and southern thrust segments, and therefore the direction of shortening must have been < 270°. Because the orientation of the folds (e.g., the Thiersee syncline; Töchterle, 2005) and faults within the Achental structure is oblique to Cretaceous shortening (e.g., Eisbacher and Brandner, 1996), many studies have offered alternative hypotheses involving multiple deformation phases and directions (e.g., Spengler, 1953; Auer, 2001; Ampferer, 1921; Fuchs, 1944; Channell et al., 1992; Channell et al., 1990; Ortner, 2003b). Although the formation of the Guffert-Unnutz-Montscheinspitze anticline and the Achental thrust is ascribed to pre-Gosau, deformation (Ortner and Gruber, 2011; Töchterle, 2005), this is no proof that the entire sigmoidal hanging wall formed during a NW direction of shortening. However, in our models we re-create the geometry of the Achental structure (including a low-angle thrust antithetic to the assumed subsurface step, and a surface expression of the hanging wall outlining the subsurface geometry) by applying shortening at 45° to the N–S trending Jurassic fault, demonstrating that a single uniform phase of oblique shortening is sufficient to create a sigmoidal shape of the hanging wall that outlines the subsurface basin geometry of the Achental structure, as depicted in Fig. 14. Our results thus agree with the hypothesis that the characteristic shape of the Achental structure formed due to forced folding at the borders of a Jurassic basin (Eisbacher and Brandner, 1995, 1996; Ortner and Gruber, 2011).

5.3 Limitations

The NCA are a salt-influenced fold-and-thrust belt with at least one (basal) décollement consisting of a pre-rift evaporitic succession. We chose to model this décollement as a relatively thin layer of iron powder-dosed silicone putty at the base of a thick, brittle sedimentary cover. However, geological settings often do not show ideal ("layer-cake") stratigraphic geometries. In salt-influenced regions, diapirs may create e.g., minibasins or flaps (e.g., Rowan et al., 2016). Using non-layer-cake geometries in physical experiments produces structures that are much different from classical thin-skinned fold-and-thrust belts (e.g., Rowan and Vendeville, 2006) and thus the classical layer-cake approach may lead to misinterpretation (Lacombe et al., 2019). In the central and eastern NCA the role of salt tectonics has been addressed by an increasing number of (recent) studies (e.g., Granado et al., 2019; Granado et al., 2021; Strauss et al., 2021; Santolaria et al., 2022; Fernández et al., 2022; Fernández et al., 2021). Resulting structural styles are highly complex and include km-scale overturned panels and missing

stratigraphy (Granado et al., 2019). The amount of salt available in salt-influenced fold-and-thrust belts controls the type of structures that can form during inversion (Hudec and Jackson, 2007; Lacombe et al., 2019). Triassic growth strata caused by

645 salt tectonics have been reported for the central and eastern NCA, and locally in the western NCA (Granado et al., 2021; Granado et al., 2019; Kilian and Ortner, 2019; Kilian et al., 2021; Ortner and Kilian, 2022; Fernández et al., 2022; Fernández et al., 2021; Strauss et al., 2021; Santolaria et al., 2022), but there are no reliable estimates on the thickness of the Haselgebirge-Reichenhall succession underneath the Achental structure. The main goal of our modelling approach was to gain insight in conditions controlling strain localization and associated folding and thrusting at pre-existing basin boundaries in an oblique

650 convergent setting. We did not aim to include the complexity of salt tectonics in our models, therefore a silicone putty has been mixed that does not favour diapir formation. Introducing Triassic salt dynamics to our models would create e.g., flaps and minibasins. Hypothetically, if the overturned panels originally were flaps onlapping salt diapirs, localisation of folding and thrusting would have been easier, as diapirs would localize thrusts. In such a case, the Jurassic basin geometry would have an even more profound effect on structures at the original basin margins.

655 Another limitation of the analogue models compared to the natural example is that we did not consider Paleogene reactivation of Cretaceous structures. Paleogene folding however, is common throughout the Achental structure and Achensee area. E.g., the Hofjoch, Blaubergalm and Seekar folds (Fig.ure 4) (Eisbacher and Brandner, 1995; Brandner and Gruber, 2011; Sausgruber, 1994b) show an orientation that corresponds to post-Cretaceous shortening. The Seekar folds are offset by the N–S striking Seekar fault, which shows dextral strike-slip movement and a P-axis that corresponds to NNE- to NE-directed

660 Paleogene shortening. Paleogene reactivation of fault planes also occurs at the west side of the Achensee (Sausgruber, 1994b). Although this post-Cretaceous reactivation may have imprinted on existing structures, we propose that the rough outlines of the Achental structure were established after Cretaceous orogeny (Fig.ure 14a).
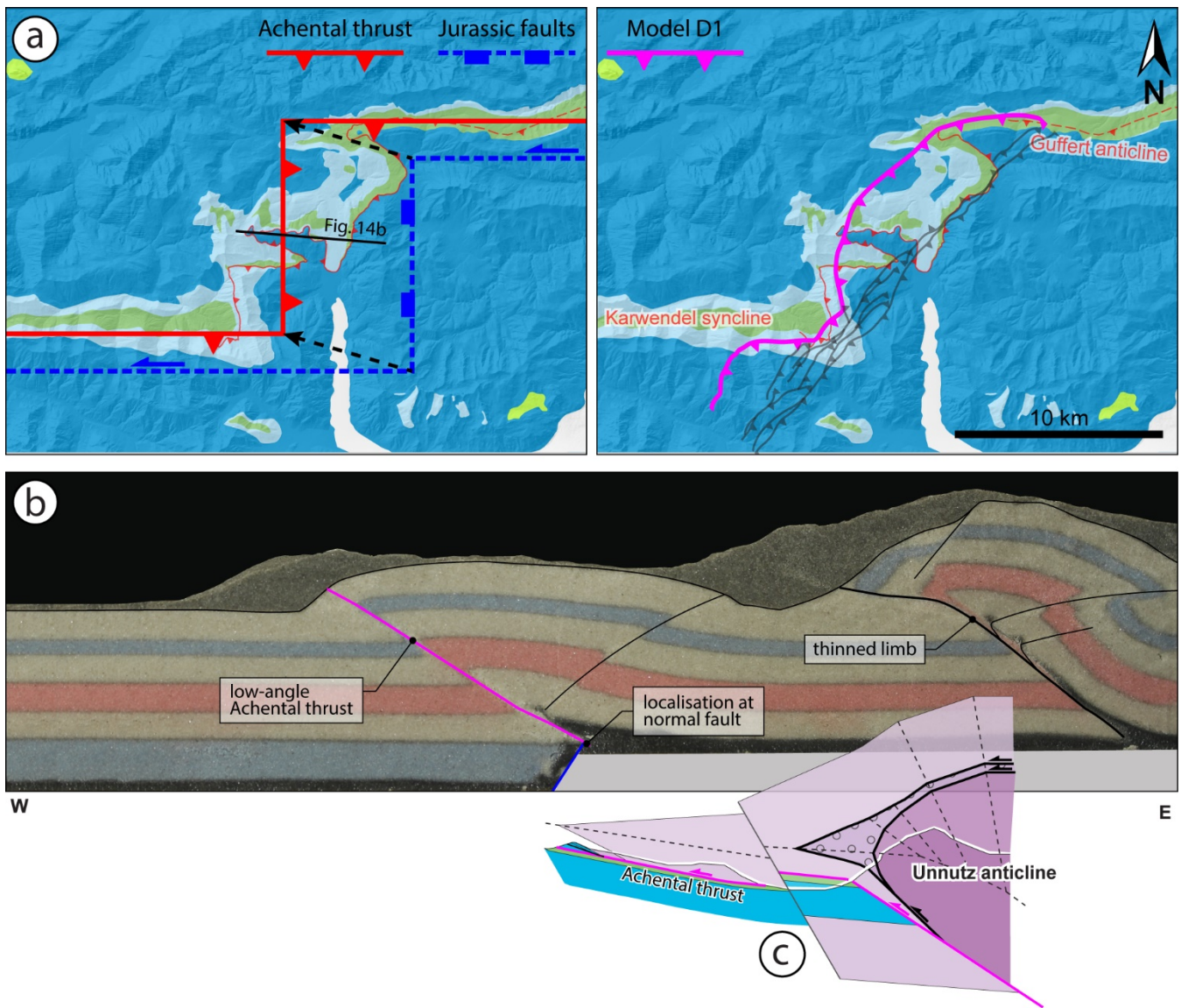
Figure 14: Summary figure showing (a) possible arrangement of Jurassic basin-bounding faults in relation to the Achental thrust (left) and overlay of inversion structures formed in analogue model D1, outlining the subsurface architecture (right). The traces of the thrusts in model D1 have not been intersected with the topography. Geological map modified after Ortner and Gruber (2011) and Ortner and Kilian (2016). For a legend of the geological map, see Fig.~~ure~~ 1. (b) shows key structural elements in a cross-section of model D1 and (c) the corresponding cross-section of the Unnutz anticline (see also Fig.~~ure~~ 5a). The Achental thrust is marked in pink. See Fig.~~ure~~ 5 for legend of lithologies.

6 Conclusions

Analogue models were used to infer favourable kinematic and mechanic conditions for the oblique inversion of a pre-existing extensional basin margin. Yet relevant for understanding deformation geometries arising from oblique basin inversion in general, the modelling results have been discussed in the frame of the Achental structure in the European Alps, which evolved from the inversion of the Jurassic Achental basin during Cretaceous and Paleogene orogenic phases. The modelling set-up was based on the assumption that the Achental basin in the subsurface of the Achental structure consists of at least (1) an approximately N–S trending, W-dipping normal fault, and (2) two E–W trending additional strike-slip faults. Furthermore, we applied a thin-skinned style of deformation and shortening at 45° to the Jurassic structures, which both characterise Cretaceous orogeny in the NCA.

The modelling results show that the basal ductile décollement of the NCA (Haselgebirge-Reichenhall succession), which separated the basement from a predominantly brittle cover, is crucial for the decoupling of the sedimentary cover. The mechanical contrast across the basin bounding normal fault then controls deformation localisation at the existing fault step. As

a result, a low-angle thrust (Achental thrust), antithetic to the Jurassic normal fault, forms at the eastern margin of the Achental basin. The hanging wall geometry of this thrust outlines the basin architecture in the subsurface, exemplifying the control of the pre-existing structural framework on structures that form during subsequent shortening. We therefore show that a single phase of Cretaceous oblique shortening at 45° to the Jurassic Achental basin axis is sufficient to form a sigmoidal geometry of the hanging wall (Achentaler Schubmasse). In a broader framework, we conclude that when shortening is applied oblique to existing basin boundaries, strain localisation leads to the formation of new thrusts along the steps formed by these structures.

Author contributions

The conceptualization of the study was done by HO and EW; Field investigations were performed by WvK, HO, AG and TS; Analogue modelling was planned and performed by WvK, EW and DS; Data preparation, analysis and visualisation were performed by WvK; WvK prepared the original draft of the manuscript with input from all co-authors; All co-authors reviewed and edited the manuscript and approved the final version.

Competing interests

At least one of the (co-)authors is a guest member of the editorial board of Solid Earth and has collaborated as a (co-)author on publications involving one of the guest editors of Solid Earth. The peer-review process was guided by an independent editor, and the authors have no other competing interests to declare.

Acknowledgements

This work was completed as part of a Master Thesis at the University of Innsbruck. The University of Innsbruck through a needs-based scholarship provided financial support covering fieldwork and travel expenses. Laboratory experiments were conducted at the TecLab of Utrecht University. Guido Schreurs, Klaus Pelz and an anonymous reviewer have provided valuable feedback, which has considerably improved the quality of this work. We sincerely thank Antoine Auzemery for assistance with the conceptualization and realization of analogue experiments, and Taco Broerse for his help with the Strainmap package, as well as fruitful discussions. We also thank Lukas Schifferle for assistance during fieldwork and digitalization. The authors thank Midland Valley for providing their Move Software in the frame of their academic software initiative and the state of Tyrol for providing high resolution hillshades.

References

Allemand, P. and Brun, J.-P.: Width of continental rifts and rheological layering of the lithosphere, Tectonophysics, 188, 63–69, https://doi.org/10.1016/0040-1951(91)90314-I, 1991.

Allen, J. and Beaumont, C.: Continental margin syn-rift salt tectonics at intermediate width margins, Basin Res., 28, 598–633, https://doi.org/10.1111/bre.12123, 2016.

Amilibia, A., McClay, K. R., Sàbat, F., Muñoz, J. A., and Roca, E.: Analogue modelling of inverted oblique rift systems, Geol. Acta, 251, https://doi.org/10.1344/105.000001395, 2005.

Ampferer, O.: Tektonische Nachbarschaft Karwendel-Sonnwendgebirge, Sitzungsberichte der Akademie der Wissenschaften in Wien, Mathematisch-Naturwissenschaftliche Klasse, 150, 181–199, 1941.

Ampferer, O.: Über NW-Beanspruchungen in den Nordalpen, Jahrbuch der Geologischen Bundesanstalt, 71, 198–202, 1921.

Ampferer, O.: Über den geologischen Zusammenhang des Karwendel- und Sonnwendgebirges, Verhandlungen der Kaiserlich-Königlichen Geologischen Reichsanstalt, 104–113, 1902.

Ampferer, O. and Heissel, G.: Geologische Karte des östlichen Karwendel und des Achensee-Gebietes, Universitätsverlag Wagner, Innsbruck, 1950.

Auer, M.: Struktur und Kinematik der nördlichen Kalkalpen im TRANSALP-Profil (Südbayern, Nordtirol), Dissertation, Universität Karlsruhe, Karlsruhe, 132 pp., 2001.

Auer, M. and Eisbacher, G. H.: Deep structure and kinematics of the Northern Calcareous Alps (TRANSALP Profile), Geol. Rundsch., 92, 210–227, https://doi.org/10.1007/s00531-003-0316-0, 2003.

Bailey, C. M., Giorgis, S., and Coiner, L.: Tectonic inversion and basement buttressing: an example from the central Appalachian Blue Ridge province, J. Struct. Geol., 24, 925–936, https://doi.org/10.1016/S0191-8141(01)00102-X, 2002.

Bechstädt, T. and Mostler, H.: Mikrofazies und Mikrofauna mitteltriadischer Beckensedimente der Nördlichen Kalkalpen Tirols, Geologisch-Paläontologische Mitteilungen Universität Innsbruck, 4, 1–74, 1974.

Beer, E.: Vergleichende tektonische Untersuchungen an zwei längsalpinen Störungen: der Achentaler Schubmasse und der Salzachstörung, Doctoral thesis, Ludwig-Maximilians-Universität München, Munich, Germany, 2003.

Bernoulli, D. and Jenkyns, H. C.: Alpine, Mediterranean, and Central Atlantic Mesozoic facies in relation to the early evolution of the Tethys, in: Modern and Ancient Geosynclinal Sedimentation, edited by: Dott, R. H. and Shaver, R. H., SEPM (Society for Sedimentary Geology), 129–160, https://doi.org/10.2110/pec.74.19.0129, 1974.

Bonini, M.: Chronology of deformation and analogue modelling of the Plio-Pleistocene 'Tiber Basin': implications for the evolution of the Northern Apennines (Italy), Tectonophysics, 285, 147–165, https://doi.org/10.1016/S0040-1951(97)00189-3, 1998.

Bonini, M., Sani, F., and Antonielli, B.: Basin inversion and contractional reactivation of inherited normal faults: A review based on previous and new experimental models, Tectonophysics, 522-523, 55–88, https://doi.org/10.1016/j.tecto.2011.11.014, 2012.

Bonini, M., Sokoutis, D., Mulugeta, G., and Katrivanos, E.: Modelling hanging wall accommodation above rigid thrust ramps, J. Struct. Geol., 22, 1165–1179, https://doi.org/10.1016/S0191-8141(00)00033-X, 2000.

Brandner, R. and Gruber, A.: Exkursion E2a - Rofangebirge, in: Arbeitstagung 2011 "Geologie des Achenseegebietes". Geologisches Kartenblatt 88, edited by: Gruber, A., Geologische Bundesanstalt, Wien, 149–167, 2011.

Brandner, R. and Poleschinski, W.: Stratigraphie und Tektonik am Kalkalpensüdrand zwischen Zirl und Seefeld in Tirol (Exkursion D am 3. April 1986), Jahresberichte und Mitteilungen des Oberrheinischen Geologischen Vereins, 68, 67–92, https://doi.org/10.1127/jmogv/68/1986/67, 1986.

Brandner, R., Lotter, M., Gruber, A., and Ortner, H.: Exkursion E3 – Achental – Bächental. Donnerstag, 22.09.2011, in: Arbeitstagung 2011 "Geologie des Achenseegebietes". Geologisches Kartenblatt 88, edited by: Gruber, A., Geologische Bundesanstalt, Wien, 199–224, 2011.

Broerse, T.: Strainmap, 2021.

Broerse, T., Krstekanić, N., Kasbergen, C., and Willingshofer, E.: Mapping and classifying large deformation from digital imagery: application to analogue models of lithosphere deformation, Geophys. J. Int., 226, 984–1017, https://doi.org/10.1093/gji/ggab120, 2021.

Brun, J.-P.: Narrow rifts versus wide rifts: inferences for the mechanics of rifting from laboratory experiments, Philos. T. R. Soc. A, 357, 695–712, https://doi.org/10.1098/rsta.1999.0349, 1999.

Brun, J.-P. and Nalpas, T.: Graben inversion in nature and experiments, Tectonics, 15, 677–687, https://doi.org/10.1029/95TC03853, 1996.

Buchanan, P. G. and McClay, K. R.: Experiments on basin inversion above reactivated domino faults, Mar. Petrol. Geol., 9, 486–500, https://doi.org/10.1016/0264-8172(92)90061-I, 1992.

Buiter, S. J. H. and Pfiffner, A. O.: Numerical models of the inversion of half-graben basins, Tectonics, 22, 1057, https://doi.org/10.1029/2002TC001417, 2003.

760   Caër, T., Souloumiac, P., Maillot, B., Leturmy, P., and Nussbaum, C.: Propagation of a fold-and-thrust belt over a basement graben, J. Struct. Geol., 115, 121–131, https://doi.org/10.1016/j.jsg.2018.07.007, 2018.

Channell, J., Brandner, R., Spieler, A., and Stoner, J. S.: Paleomagnetism and paleogeography of the Northern Calcareous Alps (Austria), Tectonics, 11, 792–810, https://doi.org/10.1029/91TC03089, 1992.

Channell, J., Brandner, R., and Spieler, A.: Mesozoic paleogeography of the Northern Calcareous Alps—Evidence from

765   paleomagnetism and facies analysis, Geology, 18, 828, https://doi.org/10.1130/0091-7613(1990)018<0828:MPOTNC>2.3.CO;2, 1990.

Cooper, M. and Warren, M. J.: Inverted fault systems and inversion tectonic settings, in: Regional Geology and Tectonics: Principles of Geologic Analysis, edited by: Scarselli, N., Adam, J., Chiarella, D., Roberts, D. G., and Bally, A. W., Elsevier, 169–204, https://doi.org/10.1016/B978-0-444-64134-2.00009-2, 2020.

770   Cotton, J. T. and Koyi, H. A.: Modeling of thrust fronts above ductile and frictional detachments: Application to structures in the Salt Range and Potwar Plateau, Pakistan, Geol. Soc. Am. Bull., 112, 351–363, https://doi.org/10.1130/0016-7606(2000)112<351:MOTFAD>2.0.CO;2, 2000.

Davis, D. M. and Engelder, T.: The role of salt in fold-and-thrust belts, Tectonophysics, 119, 67–88, https://doi.org/10.1016/0040-1951(85)90033-2, 1985.

775   Davis, D. M., Suppe, J., and Dahlen, F. A.: Mechanics of fold-and-thrust belts and accretionary wedges, J. Geophys. Res., 88, 1153, https://doi.org/10.1029/JB088iB02p01153, 1983.

Del Ventisette, C., Montanari, D., Sani, F., Bonini, M., and Corti, G.: Reply to comment by J. Wickham on "Basin inversion and fault reactivation in laboratory experiments", J. Struct. Geol., 29, 1417–1418, https://doi.org/10.1016/j.jsg.2007.05.003, 2007.

780   Del Ventisette, C., Montanari, D., Sani, F., and Bonini, M.: Basin inversion and fault reactivation in laboratory experiments, J. Struct. Geol., 28, 2067–2083, https://doi.org/10.1016/J.JSG.2006.07.012, 2006.

Deng, H., Koyi, H. A., and Zhang, J.: Modelling oblique inversion of pre-existing grabens, Geol. Soc. Sp., 487, 263–290, https://doi.org/10.1144/SP487.5, 2020.

Dombrádi, E., Sokoutis, D., Bada, G., Cloetingh, S., and Horváth, F.: Modelling recent deformation of the Pannonian

785   lithosphere: Lithospheric folding and tectonic topography, Tectonophysics, 484, 103–118, https://doi.org/10.1016/j.tecto.2009.09.014, 2010.

Donofrio, D. A., Brandner, R., and Poleschinski, W.: Conodonten der Seefeld-Formation: ein Beitrag zur Bio- und Lithostratigraphie der Hauptdolomit-Plattform (Obertrias, westliche Nördliche Kalkalpen, Tirol, Geologisch-Paläontologische Mitteilungen Universität Innsbruck, 26, 91–107, 2003.

790   Dubois, A., Odonne, F., Massonnat, G., Lebourg, T., and Fabre, R.: Analogue modelling of fault reactivation: tectonic inversion and oblique remobilisation of grabens, J. Struct. Geol., 24, 1741–1752, https://doi.org/10.1016/S0191-8141(01)00129-8, 2002.

Duffy, O. B., Dooley, T. P., Hudec, M. R., Jackson, M. P., Fernandez, N., Jackson, C. A.-L., and Soto, J. I.: Structural evolution of salt-influenced fold-and-thrust belts: A synthesis and new insights from basins containing isolated salt

795   diapirs, J. Struct. Geol., 114, 206–221, https://doi.org/10.1016/j.jsg.2018.06.024, 2018.

Eberli, G. P.: Carbonate turbidite sequences deposited in rift-basins of the Jurassic Tethys Ocean (eastern Alps, Switzerland), Sedimentology, 34, 363–388, https://doi.org/10.1111/j.1365-3091.1987.tb00576.x, 1987.

Eberli, G. P.: Die jurassischen Sedimente in den ostalpinen Decken Graubündens: Relikte eines passiven Kontinentalrandes, Thesis, ETH Zurich, 1985.

800   Eberli, G. P., Bernoulli, D., Sanders, D., and Vecsei, A.: From aggradation to progradation: The Maiella platform, Abruzzi, Italy, in: Cretaceous Carbonate Platforms, edited by: Simo, T. and Scott, R. W., 1993.

Eisbacher, G. H. and Brandner, R.: Superposed fold-thrust structures and high-angle faults, Northwestern Calcareous Alps, Austria, Eclogae Geol. Helv., 89, 553–571, 1996.

Eisbacher, G. H. and Brandner, R.: Role of high-angle faults during heteroaxial contraction, Inntal thrust sheet, Northern Calcareous Alps, western Austria, Geologisch-Paläontologische Mitteilungen Universität Innsbruck, 20, 389–406, 1995.

Eisbacher, G. H., Linzer, H.-G., and Meier, L.: A depth extrapolated structural transect across the Northern Calcareous Alps of Western Tirol, Eclogae Geol. Helv., 83, 711–725, 1990.

Epard, J.-L. and Groshong, R. H.: Kinematic model of detachment folding including limb rotation, fixed hinges and layer-parallel strain, Tectonophysics, 247, 85–103, https://doi.org/10.1016/0040-1951(94)00266-C, 1995.

Etheridge, M. A.: On the reactivation of extensional fault systems, Philos. T. R. Soc. A, 317, 179–194, https://doi.org/10.1098/rsta.1986.0031, 1986.

Fan, X., Jia, D., Yin, H., Shen, L., Liu, J., Cui, J., Sun, C., and Yang, S.: Analogue modeling of the northern Longmen Shan thrust belt (eastern margin of the Tibetan plateau) and strain analysis based on Particle Image Velocimetry, J. Asian Earth Sci., 198, 104238, https://doi.org/10.1016/j.jseaes.2020.104238, 2020.

Faupl, P. and Wagreich, M.: Late Jurassic to Eocene Palaeogeography and Geodynamic Evolution of the Eastern Alps, Mitteilungen der Österreichischen Geologischen Gesellschaft, 92, 79–94, 1999.

Fernández, O., Grasemann, B., and Sanders, D.: Deformation of the Dachstein Limestone in the Dachstein thrust sheet (Eastern Alps, Austria), Austrian J. Earth Sc., 115, 167–190, https://doi.org/10.17738/ajes.2022.0008, 2022.

Fernández, O., Habermüller, M., and Grasemann, B.: Hooked on salt: Rethinking Alpine tectonics in Hallstatt (Eastern Alps, Austria), Geology, 49, 325–329, https://doi.org/10.1130/g47981.1, 2021.

Froitzheim, N. and Manatschal, G.: Kinematics of Jurassic rifting, mantle exhumation, and passive-margin formation in the Austroalpine and Penninic nappes (eastern Switzerland), Geol. Soc. Am. Bull., 108, 1120–1133, https://doi.org/10.1130/0016-7606(1996)108<1120:KOJRME>2.3.CO;2, 1996.

Froitzheim, N., Schmid, S. M., and Conti, P.: Repeated change from crustal shortening to orogen-parallel extension in the Austroalpine units of Graubünden, https://doi.org/10.5169/seals-167471, 1994.

Fruth, I. and Scherreiks, R.: Hauptdolomit (Norian) — stratigraphy, paleogeography and diagenesis, Sedimentary Geology, 32, 195–231, https://doi.org/10.1016/0037-0738(82)90050-1, 1982.

Fuchs, A.: Untersuchungen am tektonischen Gefüge der Tiroler Alpen. II. (Kalkalpen Achensee – Kaisergebirge), Neues Jb. Miner. Abh., 88, 337–373, 1944.

Gawlick, H.-J.: Definition of the Tauglboden Formation (Oxfordian to Tithonian) in the Tauglboden Basin (Northern Calcareous Alps), Berichte des Institutes für Erdwissenschaften der Karl-Franzens-Universität Graz, 9, 2004.

Giles, K. A. and Rowan, M. G.: Concepts in halokinetic-sequence deformation and stratigraphy, Geol. Soc. Sp., 363, 7–31, https://doi.org/10.1144/SP363.2, 2012.

Golebiowski, R.: Becken und Riffe der alpinen Obertrias. Lithostratigraphie und Biofazies der Kössener Formation: Exkursionen im Jungpaläozoikum und Mesozoikum Österreichs, Österreichische Paläontologische Gesellschaft, Wien, 1991.

Gomes, C. J., Danderfer Filho, A., Posada, A. M. A., and Da Silva, A. C.: The role of backstop shape during inversion tectonics physical models, An. Acad. Bras. Ciênc., 82, 997–1012, https://doi.org/10.1590/S0001-37652010000400021, 2010.

Granado, P., Ruh, J. B., Santolaria, P., Strauss, P., and Muñoz, J. A.: Stretching and Contraction of Extensional Basins With Pre-Rift Salt: A Numerical Modeling Approach, Front. Earth Sci., 9, https://doi.org/10.3389/feart.2021.648937, 2021.

Granado, P., Roca, E., Strauss, P., Pelz, K., and Muñoz, J. A.: Structural styles in fold-and-thrust belts involving early salt structures: The Northern Calcareous Alps (Austria), Geology, 47, 51–54, https://doi.org/10.1130/G45281.1, 2019.

Graveleau, F., Malavieille, J., and Dominguez, S.: Experimental modelling of orogenic wedges: A review, Tectonophysics, 538-540, 1–66, https://doi.org/10.1016/j.tecto.2012.01.027, 2012.

845

Gruber, A.: Geological manuscript map ÖK 88 Achenkirch: Unveröff. Manuskriptkarte, Geologische Bundesanstalt, Wien, 2011.

Gruber, A., Lotter, M., and Geologische Bundesanstalt: Erläuterungen zu Blatt 88 Achenkirch, Geologische Karte der Republik Österreich [Geologische Karte Österreich / Erläuterungen] Erläuterungen, Geologische Bundesanstalt, Wien,

850   2022.

Gümbel, C. W.: Geognostische Beschreibung des bayerischen Alpengebirges und seines Vorlandes, Perthes, Gotha, 950 pp., 1861.

Haas, J., Kovács, S., Krystyn, L., and Lein, R.: Significance of Late Permian-Triassic facies zones in terrane reconstructions in the Alpine-North Pannonian domain, Tectonophysics, 242, 19–40, https://doi.org/10.1016/0040-1951(94)00157-5,

855   1995.

Héja, G., Ortner, H., Fodor, L., Németh, A., and Kövér, S.: Modes of Oblique Inversion: A Case Study from the Cretaceous Fold and Thrust Belt of the Western Transdanubian Range (TR), West Hungary, Tectonics, 41, https://doi.org/10.1029/2021TC006728, 2022.

Homza, T. X. and Wallace, W. K.: Geometric and kinematic models for detachment folds with fixed and variable

860   detachment depths, J. Struct. Geol., 17, 575–588, https://doi.org/10.1016/0191-8141(94)00077-D, 1995.

Hubbert, M. K.: Theory of scale models as applied to the study of geologic structures, Geol. Soc. Am. Bull., 48, 1459–1520, https://doi.org/10.1130/GSAB-48-1459, 1937.

Hudec, M. R. and Jackson, M. P.: Terra infirma: Understanding salt tectonics, Earth-Sci. Rev., 82, 1–28, https://doi.org/10.1016/j.earscirev.2007.01.001, 2007.

865 Jamison, W. R.: Geometric analysis of fold development in overthrust terranes, J. Struct. Geol., 9, 207–219, https://doi.org/10.1016/0191-8141(87)90026-5, 1987.

Jaumé, S. C. and Lillie, R. J.: Mechanics of the Salt Range-Potwar Plateau, Pakistan: A fold-and-thrust belt underlain by evaporites, Tectonics, 7, 57–71, https://doi.org/10.1029/TC007i001p00057, 1988.

Jerz, H.: Untersuchungen über Stoffbestand, Bildungsbedingungen und Paläogeographie der Raibler Schichten zwischen

870   Lech und Inn (Nördl. Kalkalpen), Geologica Bavarica, 56, 3–100, 1966.

Josep Poblet, K. M.: Geometry and Kinematics of Single-Layer Detachment Folds, AAPG Bull., 80, https://doi.org/10.1306/64ED8CA0-1724-11D7-8645000102C1865D, 1996.

Kilian, S.: Bericht 2012 über geologische und strukturgeologische Aufnahmen im Karwendelgebirge auf Blatt 2223 Innsbruck und auf Blatt 2217 Hinterriß, Jahrbuch der Geologischen Bundesanstalt, 153, 411–417, 2013.

875 Kilian, S. and Ortner, H.: Structural evidence of in-sequence and out-of-sequence thrusting in the Karwendel mountains and the tectonic subdivision of the western Northern Calcareous Alps, Austrian J. Earth Sc., 112, 62–83, https://doi.org/10.17738/ajes.2019.0005, 2019.

Kilian, S., Ortner, H., and Schneider-Muntau, B.: Buckle folding in the Northern Calcareous Alps - Field observations and numeric experiments, J. Struct. Geol., 150, 104416, https://doi.org/10.1016/j.jsg.2021.104416, 2021.

880 Kley, J., Rosello, E. A., Monaldi, C. R., and Habighorst, B.: Seismic and field evidence for selective inversion of Cretaceous normal faults, Salta rift, northwest Argentina, Tectonophysics, 399, 155–172, https://doi.org/10.1016/J.TECTO.2004.12.020, 2005.

Konstantinovskaya, E. A., Harris, L. B., Poulin, J., and Ivanov, G. M.: Transfer zones and fault reactivation in inverted rift basins: Insights from physical modelling, Tectonophysics, 441, 1–26, https://doi.org/10.1016/j.tecto.2007.06.002, 2007.

885 Koopman, A., Speksnijder, A., and Horsfield, W. T.: Sandbox model studies of inversion tectonics, Tectonophysics, 137, 379–388, https://doi.org/10.1016/0040-1951(87)90329-5, 1987.

Krainer, K., Lucas, S. G., and Strasser, M.: Vertebrate Fossils from the Northalpine Raibl Beds, Western Northern Calcareous Alps, Tyrol (Austria), Austrian J. Earth Sc., 104, 97–106, 2011.

Krstekanić, N., Willingshofer, E., Matenco, L., Toljić, M., and Stojadinovic, U.: The influence of back-arc extension

890   direction on the strain partitioning associated with continental indentation: Analogue modelling and implications for the Circum-Moesian Fault System of South-Eastern Europe, J. Struct. Geol., 159, 104599, https://doi.org/10.1016/j.jsg.2022.104599, 2022.

Krstekanić, N., Willingshofer, E., Broerse, T., Matenco, L., Toljić, M., and Stojadinovic, U.: Analogue modelling of strain partitioning along a curved strike-slip fault system during backarc-convex orocline formation: Implications for the

895   Cerna-Timok fault system of the Carpatho-Balkanides, J. Struct. Geol., 149, 104386, https://doi.org/10.1016/j.jsg.2021.104386, 2021.

Lackschewitz, K. S., Grützmacher, U., and Henrich, R.: Paleoceanography and rotational block faulting in the Jurassic carbonate series of the Chiemgau Alps (Bavaria), Facies, 24, 1–23, https://doi.org/10.1007/BF02536838, 1991.

Lacombe, O., Mazzoli, S., Hagke, C. von, Rosenau, M., Fillon, C., and Granado, P.: Style of deformation and tectono-

900   sedimentary evolution of fold-and-thrust belts and foreland basins: From nature to models, Tectonophysics, 767, 228163, https://doi.org/10.1016/j.tecto.2019.228163, 2019.

Laubscher, H. P.: The eastern Jura: Relations between thin-skinned and basement tectonics, local and regional, Geol. Rundsch., 75, 535–553, https://doi.org/10.1007/BF01820630, 1986.

Lee, A. R. and Warren, J. B.: A coni-cylindrical viscometer for measuring the visco-elastic characteristics of highly viscous

905   liquids, J. Sci. Instrum., 17, 63–67, https://doi.org/10.1088/0950-7671/17/3/303, 1940.

Leever, K. A., Gabrielsen, R. H., Faleide, J. I., and Braathen, A.: A transpressional origin for the West Spitsbergen fold-and-thrust belt: Insight from analog modeling, Tectonics, 30, n/a-n/a, https://doi.org/10.1029/2010TC002753, 2011.

Lein, R.: Evolution of the Northern Calcareous Alps during Triassic times, in: Geodynamics of the Eastern Alps, edited by: Flügel, H. W. and Faupl, P., Deuticke, Wien, 85–102, 1987.

910   Leitner, C. and Neubauer, F.: Tectonic significance of structures within the salt deposits Altaussee and Berchtesgaden–Bad Dürrnberg, Northern Calcareous Alps, Austrian J. Earth Sc., 104, 2–21, 2011.

Lemoine, M., Bas, T., Arnaud-Vanneau, A., Arnaud, H., Dumont, T., Gidon, M., Bourbon, M., Graciansky, P.-C. de, Rudkiewicz, J.-L., Megard-Galli, J., and Tricart, P.: The continental margin of the Mesozoic Tethys in the Western Alps, Mar. Petrol. Geol., 3, 179–199, https://doi.org/10.1016/0264-8172(86)90044-9, 1986.

915   Lipold, M. W.: Der Salzberg am Dürrnberg nächst Hallein, Jahrbuch der Kaiserlich-Königlichen Geologischen Reichsanstalt, 5, 590–610, 1854.

Manger, G. E.: Porosity and bulk density of sedimentary rocks., Geological Survey Bulletin, 1144-E, 1963.

Martin, J. and Mercier, E.: Heritage distensif et structuration chevauchante dans une chaine de couverture; apport de l'equilibrage par modelisation geometrique dans le Jura nord-occidental, B. Soc. Geol. Fr., 167, 101–110, 1996.

920   Merle, O. and Abidi, N.: Approche experimentale du fonctionnement des rampes emergentes, B. Soc. Geol. Fr., 166, 439–450, https://doi.org/10.2113/gssgfbull.166.5.439, 1995.

Mitra, S.: Structural models of faulted detachment folds, AAPG Bull., 86, https://doi.org/10.1306/61EEDD3C-173E-11D7-8645000102C1865D, 2002.

Mojsisovics, E. von: Beiträge zur topischen Geologie der Alpen, Jahrbuch der Geologischen Reichsanstalt, 21, 189–210,

925   1871.

Molnar, N. and Buiter, S. J. H.: Analogue modelling of the inversion of multiple extensional basins in foreland fold-and-thrust belts, Solid Earth, 14, 213–235, https://doi.org/10.5194/se-14-213-2023, 2023.

Mooney, M. and Ewart, R. H.: The Conicylindrical Viscometer, Physics, 5, 350–354, https://doi.org/10.1063/1.1745219, 1934.

930 Morley, C. K.: Fold-generated imbricates: examples from the Caledonides of Southern Norway, J. Struct. Geol., 16, 619–631, https://doi.org/10.1016/0191-8141(94)90114-7, 1994.

Müller-Jungbluth, W.-U.: Sedimentary Petrologic Investigation of the Upper Triassic "Hauptdolomit" of the Lechtaler Alps, Tyrol, Austria, in: Recent Developments in Carbonate Sedimentology in Central Europe, edited by: Müller, G. and Friedman, G. M., Springer Berlin Heidelberg, Berlin, Heidelberg, 228–239, 1968.

935 Mulugeta, G.: Modelling the geometry of Coulomb thrust wedges, J. Struct. Geol., 10, 847–859, https://doi.org/10.1016/0191-8141(88)90099-5, 1988.

Nagel, K.-H.: Der Bau der Thiersee- und Karwendelmulde (Tirol), Geotektonische Forschungen, 48, Stuttgart, 1975.

Nagel, K.-H., Schütz, K.-I., Schütz, S., Wilmers, W., and Zeil, W.: Die geodynamische Entwicklung der Thiersee- und der Karwendelmulde (Nördliche Kalkalpen), Geol. Rundsch., 65, 536–557, 1976.

940 Nielsen, S. B. and Hansen, D. L.: Physical explanation of the formation and evolution of inversion zones and marginal troughs, Geology, 28, 875, https://doi.org/10.1130/0091-7613(2000)28<875:PEOTFA>2.0.CO;2, 2000.

Ortner, H.: Field trip 4 Deep water sedimentation on top of a growing orogenic wedge - interaction of thrusting, erosion and deposition in the Cretaceous Northern Calcareous Alps, Geo.Alp, 13, 141–182, 2016.

Ortner, H.: Local and far field stress-analysis of brittle deformation in the western part of the Northern Calcareous Alps,
945 Austria, Geologisch-Paläontologische Mitteilungen Universität Innsbruck, 26, 109–136, 2003a.

Ortner, H.: Cretaceous thrusting in the western part of the Northern Calcareous Alps (Austria) - evidences from synorogenic sedimentation and structural data, Mitteilungen der Österreichischen Geologischen Gesellschaft, 94, 63–77, 2003b.

Ortner, H.: Growing folds and sedimentation of the Gosau Group, Muttekopf, Northern Calcareous Alps, Austria, Geol. Rundsch., 90, 727–739, https://doi.org/10.1007/s005310000182, 2001.

950 Ortner, H. and Sieberer, A.-K.: From foreland thrust belt to accretionary wedge: Synorogenic sediments monitor a changing geodynamic setting in the Northern Calcareous Alps of the European Eastern Alps, EGU General Assembly 2022, Vienna, Austria, 23–27 May 2022, EGU22-11281, https://doi.org/10.5194/egusphere-egu22-11281, 2022.

Ortner, H. and Kilian, S.: Thrust tectonics in the Wetterstein and Mieming mountains, and a new tectonic subdivision of the Northern Calcareous Alps of Western Austria and Southern Germany, Geol. Rundsch., 111, 543–571,
955 https://doi.org/10.1007/s00531-021-02128-3, 2022.

Ortner, H. and Kilian, S.: Sediment creep on slopes in pelagic limestones: Upper Jurassic of Northern Calcareous Alps, Austria, Sedimentary Geology, 344, 350–363, https://doi.org/10.1016/J.SEDGEO.2016.03.013, 2016.

Ortner, H. and Gruber, A.: 3D-Geometrie der Strukturen zwischen Karwendel-Synklinale und Thiersee-Synklinale, in: Arbeitstagung 2011 "Geologie des Achenseegebietes". Geologisches Kartenblatt 88, edited by: Gruber, A., Geologische
960 Bundesanstalt, Wien, 51–67, 2011.

Ortner, H. and Gaupp, R.: Synorogenic sediments of the western Northern Calcareous Alps, Geo.Alp, 4, 133–148, 2007.

Ortner, H., Kositz, A., Willingshofer, E., and Sokoutis, D.: Geometry of growth strata in a transpressive fold belt in field and analogue model: Gosau Group at Muttekopf, Northern Calcareous Alps, Austria, Basin Res., 28, 731–751, https://doi.org/10.1111/bre.12129, 2016.

965 Ortner, H., Ustaszewski, M., and Rittner, M.: Late Jurassic tectonics and sedimentation: breccias in the Unken syncline, central Northern Calcareous Alps, Swiss J. Geosci., 101, 55–71, https://doi.org/10.1007/s00015-008-1282-0, 2008.

Persson, K. S. and Sokoutis, D.: Analogue models of orogenic wedges controlled by erosion, Tectonophysics, 356, 323–336, https://doi.org/10.1016/S0040-1951(02)00443-2, 2002.

Quenstedt, W.: Studien in der Überschiebungszone von Achenkirch, Zeitschrift der Deutschen Geologischen Gesellschaft,
970 85, 459–461, 1933.

Ramberg, H.: Gravity, deformation and the earth's crust: In theory, experiments and geological application, 2nd ed., Academic Press, London, 1981.

Riedel, P.: Facies and development of the 'wilde kirche' reef complex (Rhaetian, Upper Triassic, Karwendelgebirge, Austria), Facies, 18, 205–217, https://doi.org/10.1007/BF02536800, 1988.

975 Rodgers, J.: Evolution of Thought on Structure of Middle and Southern Appalachians, AAPG Bull., 33, https://doi.org/10.1306/3D933E00-16B1-11D7-8645000102C1865D, 1949.

Rowan, M. G. and Vendeville, B. C.: Foldbelts with early salt withdrawal and diapirism: Physical model and examples from the northern Gulf of Mexico and the Flinders Ranges, Australia, Mar. Petrol. Geol., 23, 871–891, https://doi.org/10.1016/j.marpetgeo.2006.08.003, 2006.

980 Rowan, M. G., Giles, K. A., Hearon IV, T. E., and Fiduk, J. C.: Megaflaps adjacent to salt diapirs, AAPG Bull., 100, 1723–1747, https://doi.org/10.1306/05241616009, 2016.

Rüffer, T. and Zühlke, R.: Sequence Stratigraphy and Sea-Level Changes in the Early to Middle Triassic of the Alps: A Global Comparison, in: Sequence Stratigraphy and Depositional Response to Eustatic, Tectonic and Climatic Forcing, edited by: Haq, B., Kluwer, Dordrecht, 161–207, 1995.

985 Santolaria, P., Granado, P., Wilson, E. P., Matteis, M. de, Ferrer, O., Strauss, P., Pelz, K., König, M., Oteleanu, A. E., Roca, E., and Muñoz, J. A.: From Salt-Bearing Rifted Margins to Fold-And-Thrust Belts. Insights from Analog Modeling and Northern Calcareous Alps Case Study, Tectonics, 41, https://doi.org/10.1029/2022TC007503, 2022.

Sassi, W., Colletta, B., Balé, P., and Paquereau, T.: Modelling of structural complexity in sedimentary basins: The role of pre-existing faults in thrust tectonics, Tectonophysics, 226, 97–112, https://doi.org/10.1016/0040-1951(93)90113-X, 990 1993.

Sausgruber, T.: Bericht 1993 über geologische Aufnahmen in den Nördlichen Kalkalpen auf Blatt 88 Achenkirch, Jahrbuch der Geologischen Bundesanstalt, 137, 469, 1994a.

Sausgruber, T.: Jurabeckenentwicklung nördlich vom Achensee und deren Folgen bei der alpidischen Kompressionstektonik, Diploma thesis, Leopold-Franzens Universität Innsbruck, Innsbruck, 133 pp., 1994b.

995 Schmid, S. M., Bernoulli, D., Fügenschuh, B., Matenco, L., Schefer, S., Schuster, R., Tischler, M., and Ustaszewski, K.: The Alpine-Carpathian-Dinaridic orogenic system: correlation and evolution of tectonic units, Swiss J. Geosci., 101, 139–183, https://doi.org/10.1007/s00015-008-1247-3, 2008.

Schmid, S. M., Fügenschuh, B., Kissling, E., and Schuster, R.: Tectonic map and overall architecture of the Alpine orogen, Eclogae Geol. Helv., 97, 93–117, https://doi.org/10.1007/s00015-004-1113-x, 2004.

1000 Schmid, S. M., Pfiffner, A. O., Froitzheim, N., Schönborn, G., and Kissling, E.: Geophysical-geological transect and tectonic evolution of the Swiss-Italian Alps, Tectonics, 15, 1036–1064, https://doi.org/10.1029/96TC00433, 1996.

Schuster, R., Daurer, A., Krenmayr, H. G., Linner, M., Mandl, G. W., Pestal, G., and Reitner, J. M.: Rocky Austria: The Geology of Austria - brief and colourful, 3. Auflage, revidierte Ausgabe, GeoSphere Austria, Wien, 80 pp., 2019.

Schütz, K.-I.: Die Aptychenschichten der Thiersee- und der Karwendel-Mulde, Geotektonische Forschungen, 57, 1–84, 1005 1979.

Sibson, R. H.: Selective fault reactivation during basin inversion: potential for fluid redistribution through fault-valve action, Geol. Soc. Sp., 88, 3–19, https://doi.org/10.1144/GSL.SP.1995.088.01.02, 1995.

Sieberer, A.-K., Willingshofer, E., Klotz, T., Ortner, H., and Pomella, H.: Inversion of extensional basins parallel and oblique to their boundaries: inferences from analogue models and field observations from the Dolomites Indenter, 1010 European eastern Southern Alps, Solid Earth, 14, 647–681, https://doi.org/10.5194/se-14-647-2023, 2023.

Smit, J. H. W.: Brittle-ductile coupling in thrust wedges and continental transforms, Doctoral thesis, VU Amsterdam & Université de Rennes, Amsterdam, Rennes, 2005.

Smit, J. H. W., Brun, J.-P., and Sokoutis, D.: Deformation of brittle-ductile thrust wedges in experiments and nature, J. Geophys. Res., 108, https://doi.org/10.1029/2002JB002190, 2003.

1015   Snidero, M., Muñoz, J. A., Carrera, N., Butillé, M., Mencos, J., Motamedi, H., Piryaei, A., and Sàbat, F.: Temporal evolution of the Darmadan salt diapir, eastern Fars region, Iran, Tectonophysics, 766, 115–130, https://doi.org/10.1016/j.tecto.2019.06.006, 2019.

Sokoutis, D., Burg, J.-P., Bonini, M., Corti, G., and Cloetingh, S.: Lithospheric-scale structures from the perspective of analogue continental collision, Tectonophysics, 406, 1–15, https://doi.org/10.1016/J.TECTO.2005.05.025, 2005.

1020   Sokoutis, D., Bonini, M., Medvedev, S., Boccaletti, M., Talbot, C. J., and Koyi, H. A.: Indentation of a continent with a built-in thickness change: experiment and nature, Tectonophysics, 320, 243–270, https://doi.org/10.1016/S0040-1951(00)00043-3, 2000.

Spengler, E.: Versuch einer Rekonstruktion des Ablagerungsraumes der nördlichen Kalkalpen (2. Teil, Mittelabschnitt), Jahrbuch der Geologischen Bundesanstalt, 99, 1–74, 1956.

1025   Spengler, E.: Versuch einer Rekonstruktion des Ablagerungsraumes der nördlichen Kalkalpen (1. Teil, Westabschnitt), Jahrbuch der Geologischen Bundesanstalt, 96, 1–64, 1953.

Spieler, A.: Geological manuscript map, 1995.

Spieler, A.: Bericht 1993 über geologische Aufnahmen in den Nördlichen Kalkalpen auf Blatt 88 Achenkirch, Jahrbuch der Geologischen Bundesanstalt, 137, 474–475, 1994.

1030   Spieler, A. and Brandner, R.: Vom Jurassischen Pull-apart Becken zur Westüberschiebung der Achentaler Schubmasse (Tirol, Österreich), Geologisch-Paläontologische Mitteilungen Universität Innsbruck, 16, 191–194, 1989.

Spötl, C.: The Alpine Haselgebirge Formation, Northern Calcareous Alps (Austria): Permo-Scythian evaporites in an alpine thrust system, Sedimentary Geology, 65, 113–125, https://doi.org/10.1016/0037-0738(89)90009-2, 1989.

Stampfli, G., Mosar, J., Marquer, D., Marchant, R., Baudin, T., and Borel, G.: Subduction and obduction processes in the

1035   Swiss Alps, Tectonophysics, 296, 159–204, https://doi.org/10.1016/S0040-1951(98)00142-5, 1998.

Storti, F. and Salvini, F.: Progressive Rollover Fault-Propagation Folding: A Possible Kinematic Mechanism to Generate Regional-Scale Recumbent Folds in Shallow Foreland Belts, AAPG Bull., 80, https://doi.org/10.1306/64ED8782-1724-11D7-8645000102C1865D, 1996.

Strauss, P., Granado, P., and Muñoz, J. A.: Subsidence analysis of salt tectonics-driven carbonate minibasins (Northern

1040   Calcareous Alps, Austria), Basin Res., 33, 968–990, https://doi.org/10.1111/bre.12500, 2021.

Stüwe, K. and Schuster, R.: Initiation of subduction in the Alps: Continent or ocean?, Geology, 38, 175–178, https://doi.org/10.1130/G30528.1, 2010.

Suppe, J.: Principles of structural geology, Prentice-Hall, Englewood Cliffs, New Jersey, 1985.

Suppe, J. and Medwedeff, D. A.: Geometry and kinematics of fault-propagation folding, Eclogae Geol. Helv., 83, 409–454,

1045   available at: https://api.semanticscholar.org/CorpusID:131023185, 1990.

Tavarnelli, E.: The effects of pre-existing normal faults on thrust ramp development: An example from the northern Apennines, Italy, Geol. Rundsch., 85, 363–371, https://doi.org/10.1007/BF02422241, 1996.

Thielicke, W.: The Flapping Flight of Birds - Analysis and Application, PhD thesis, Rijksuniversiteit Groningen, Groningen, Netherlands, 2014.

1050   Thielicke, W. and Sonntag, R.: Particle Image Velocimetry for MATLAB: Accuracy and enhanced algorithms in PIVlab, Journal of Open Research Software, 9, 12, https://doi.org/10.5334/jors.334, 2021.

Thielicke, W. and Stamhuis, E. J.: PIVlab – Towards User-friendly, Affordable and Accurate Digital Particle Image Velocimetry in MATLAB, Journal of Open Research Software, 2, https://doi.org/10.5334/jors.bl, 2014.

Thorwart, M., Dannowski, A., Grevemeyer, I., Lange, D., Kopp, H., Petersen, F., Crawford, W. C., and Paul, A.: Basin

1055   inversion: reactivated rift structures in the central Ligurian Sea revealed using ocean bottom seismometers, Solid Earth, 12, 2553–2571, https://doi.org/10.5194/se-12-2553-2021, 2021.

Töchterle, A.: Tektonische Entwicklungsgeschichte des Südteiles der Nördlichen Kalkalpen entlang der TRANSALP-Tiefenseismik anhand bilanzierter Profile, Diploma thesis, Leopold-Franzens Universität Innsbruck, Innsbruck, 2005.

Tong, H. and an Yin: Reactivation tendency analysis: A theory for predicting the temporal evolution of preexisting weakness under uniform stress state, Tectonophysics, 503, 195–200, https://doi.org/10.1016/j.tecto.2011.02.012, 2011.

Tron, V. and Brun, J.-P.: Experiments on oblique rifting in brittle-ductile systems, Tectonophysics, 188, 71–84, https://doi.org/10.1016/0040-1951(91)90315-J, 1991.

Turner, J. P. and Williams, G. A.: Sedimentary basin inversion and intra-plate shortening, Earth-Sci. Rev., 65, 277–304, 2004.

Ulrich, R.: Die Entwicklung der ostalpinen Juraformation im Vorkarwendel zwischen Mittenwald und Achensee, Geologica Bavarica, 41, 99–151, 1960.

van Gelder, I. E., Willingshofer, E., Sokoutis, D., and Cloetingh, S.: The interplay between subduction and lateral extrusion: A case study for the European Eastern Alps based on analogue models, Earth Planet. Sc. Lett., 472, 82–94, https://doi.org/10.1016/j.epsl.2017.05.012, 2017.

Wallace, W. K. and Homza, T. X.: Detachment folds versus fault-propagation folds, and their truncation by thrust faults, in: Thrust tectonics and hydrocarbon systems, edited by: McClay, K. R., 324–355, 2004.

Weijermars, R.: Polydimethylsiloxane flow defined for experiments in fluid dynamics, Appl. Phys. Lett., 48, 109–111, https://doi.org/10.1063/1.97008, 1986a.

Weijermars, R.: Finite strain of laminar flows can be visualized in SGM36-polymer, Naturwissenschaften, 73, 33–34, https://doi.org/10.1007/BF01168803, 1986b.

Weijermars, R.: Flow behaviour and physical chemistry of bouncing putties and related polymers in view of tectonic laboratory applications, Tectonophysics, 124, 325–358, https://doi.org/10.1016/0040-1951(86)90208-8, 1986c.

Weijermars, R. and Schmeling, H.: Scaling of Newtonian and non-Newtonian fluid dynamics without inertia for quantitative modelling of rock flow due to gravity (including the concept of rheological similarity), Physics of the Earth and Planetary Interiors, 43, 316–330, https://doi.org/10.1016/0031-9201(86)90021-X, 1986.

Weijermars, R., Jackson, M. P., and Vendeville, B. C.: Rheological and tectonic modeling of salt provinces, Tectonophysics, 217, 143–174, https://doi.org/10.1016/0040-1951(93)90208-2, 1993.

Weissert, H. J. and Bernoulli, D.: A transform margin in the Mesozoic Tethys: evidence from the Swiss Alps, Geol. Rundsch., 74, 665–679, https://doi.org/10.1007/BF01821220, 1985.

Wickham, J.: Comment on "Basin inversion and fault reactivation in laboratory experiments", J. Struct. Geol., 29, 1414–1416, https://doi.org/10.1016/j.jsg.2007.05.002, 2007.

Willingshofer, E., Sokoutis, D., Beekman, F., Schönebeck, J.-M., Warsitzka, M., and Rosenau, M.: Ring shear test data of feldspar sand and quartz sand used in the Tectonic Laboratory (TecLab) at Utrecht University for experimental Earth Science applications, 2018.

Willingshofer, E., Sokoutis, D., and Burg, J.-P.: Lithospheric-scale analogue modelling of collision zones with a pre-existing weak zone, Geol. Soc. Sp., 243, 277–294, https://doi.org/10.1144/gsl.sp.2005.243.01.18, 2005.

Willingshofer, E., Neubauer, F., and Cloetingh, S.: The significance of Gosau-type basins for the late cretaceous tectonic history of the Alpine-Carpathian belt, Physics and Chemistry of the Earth, Part A: Solid Earth and Geodesy, 24, 687–695, https://doi.org/10.1016/S1464-1895(99)00100-3, 1999.

Yagupsky, D. L., Cristallini, E. O., Fantín, J., Valcarce, G. Z., Bottesi, G., and Varadé, R.: Oblique half-graben inversion of the Mesozoic Neuquén Rift in the Malargüe Fold and Thrust Belt, Mendoza, Argentina: New insights from analogue models, J. Struct. Geol., 30, 839–853, https://doi.org/10.1016/j.jsg.2008.03.007, 2008.

Zorlu, J.: Sedimentpetrographische und geochemische Untersuchungen an unterschiedlich überprägten Triasdolomiten der Ost- und Südalpen, Doctoral thesis, Ruhr-Universität Bochum, Bochum, 2007.

1100   Zwaan, F., Schreurs, G., Buiter, S. J. H., Ferrer, O., Reitano, R., Rudolf, M., and Willingshofer, E.: Analogue modelling of basin inversion: a review and future perspectives, Solid Earth, 13, 1859–1905, https://doi.org/10.5194/se-13-1859-2022, 2022.